NON-CRYOGENIC HIGH DUTY CYCLE ELECTRON LINEAR ACCELERATORS*

J. Haimson
Massachusetts Institute of Technology
Cambridge, Massachusetts

1. Introduction

In order to reduce the count-rate of accidental coincidences and obtain more meaningful data from which the reaction kinematics of electron scattering experiments can be specified, it is necessary that beam duty factors be much higher than that normally provided by conventional linear accelerators (0.1 percent) and preferably comparable to that of electron synchrotrons. Also, since the nuclear cross sections of interest are small, it is desirable that beams of high intensity with good spatial and energy resolution be available. The Saclay[1,2] and MIT[3] linear accelerators were designed to meet the need for this type of high intensity, high duty intermediate energy machine.

In the early part of this decade, when detailed design studies were first undertaken to investigate intermediate energy linear accelerators having duty factors 10 to 100 times greater than those currently in service, emphasis was placed on extending the existing art rather than furthering the development of cryogenic techniques. Although superconductivity held a promise of achieving the ultimate in high duty factor performance, namely, cw operation, several considerations of a technical and scheduling nature favored the adoption of non-cryogenic methods. The following factors were paramount in influencing this decision: (a) a desire for nuclear physics experimental programs to be fully operational by 1969 - 1970; (b) the need to transfer approximately 100 kW of average power from the RF fields to the electron beam while maintaining a large fraction of the total current within a spectrum width of several tenths of 1 percent; (c) pulsed microwave generators with demonstrated average power outputs of greater than 100 kW at high duty factors were available over a wide range of frequencies; (d) the need, with a cryogenic system, for extreme stability of the microwave structure and RF source; and (e) possible deterioration of the superconducting state due to surface irregularities, contaminants, field emission and beam spillage, leading to instabilities and broadening of the beam energy spectra. The recent achievements and future prospects of high duty superconducting electron linear accelerators have been reviewed elsewhere,[4,5] and the concepts presented in this paper refer only to high duty factor systems which utilize normal disc loaded traveling wave structures designed to operate over a wide dynamic range of peak RF power to provide narrow energy spectra, low emittance beams of high intensity.

2. General Considerations

In principle, a high duty cycle pulsed system can be readily provided by utilizing RF generators which are capable of maintaining a high level of average power while operating at reduced values of peak power. For example, an RF duty factor of 0.125 percent, as obtained with a conventional accelerator driven by klystrons having power outputs of 20 MW peak and 24 kW average, may be compared with the substantially increased factor of 2 percent as furnished by RF tubes rated at 4 MW peak and 80 kW average. Additionally, in acknowledging the narrow pass-band characteristic of the accelerating structure, klystrons can be designed to operate at constant gain and conversion efficiency over a relatively wide range of peak power. Thus, for the above example, a reduction in peak power from 4 to 1 MW while maintaining an average power of 80 kW would provide a maximum RF duty cycle of 8 percent. Adoption of this technique, however, imposes unusual technical and economic restrictions on the system design because of inherent low accelerating field gradients and high levels of power dissipation. (Typically, the field gradient will be 10 to 30 percent of that normally present in a linear accelerator designed for 0.1 percent duty.) Since the zero-loaded beam energy gain through a waveguide section can be expressed as $V_0 = (r\ell\Delta P_0)^{1/2}$, where $\Delta P_0 = P_0[1-\exp(-2\tau)]$, for low values of input peak RF power (P_0) there is a design tendency to compensate against energy loss by maximizing the unit length shunt impedance (r), the length of the section (ℓ), and the power loss (ΔP_0) by increasing the waveguide voltage attenuation parameter (τ). For some systems, this tendency is emphasized further owing to strong economic arguments which favor multiple waveguide connections per klystron.

2.1 Waveguide Attenuation

The choice of a practical maximum value for the waveguide attenuation depends primarily on the required conversion efficiency and the tolerable maximum phase sensitivity. These factors are in turn related to, and sometimes modified by, the cost of providing a suitable high volume, high velocity, temperature regulated water cooling system. High current linear accelerators, operating with steady-state peak current levels of several amperes, require attenuation parameters as low as 0.1 - 0.05 neper[6] in order to demonstrate conversion efficiencies in the range of 90 - 95 percent. Waveguide designs of this type invariably satisfy even the most stringent requirements for system phase stability, because of the low phase sensitivity associated with reduced attenuation structures. With high duty cycle machines and light beam loading, however, the need to maximize energy is more important than the attainment of high conversion efficiency, and there is a tendency for the attenuation parameter to be increased up to a maximum value consistent with the requirements of frequency, temperature and phase stability. For light beam loading conditions, some guidance in determining this value can be obtained from the simple expression $\Delta\theta = 2\tau Q\Delta f/f$ which relates waveguide phase shift ($\Delta\theta$) to change in frequency (Δf) for a given attenuation parameter and Q. As an example, consider a typical $2\pi/3$ mode, 2856 MHz waveguide having an average unloaded Q of 13,000 and a phase velocity equal to the speed of light. Then in order to limit the waveguide phase shift to, say, 2 degrees for a 4.8 kHz change in frequency (the equivalent

of 0.1^{o}C change in temperature of the waveguide) the attenuation parameter must not exceed 0.82 neper. The Fig. 1 graphs illustrate the attenuation dependent phase shifts caused by a 10 kHz change in frequency for $2\pi/3$ mode structures and several design frequencies.

Owing to the excellent long term frequency stability demonstrated by modern crystal controlled solid state RF exciter systems (less than 300 Hz), the degree of success in achieving a desired phase stability for a given large value of attenuation parameter depends crucially on the design of the waveguide water cooling and temperature control system. Although maintaining the effective temperature of the waveguide within 0.1^{o}C is a difficult task with high duty factor machines, due to wide variations and high levels of heat dissipation, the accurate location of a waveguide metal temperature sensor can enable automatic temperature-phase compensation to be obtained for a wide range of operational conditions. This concept involves aspects of waveguide construction and heat transfer as well as metal temperature sensing and beam loading effects and has been discussed elsewhere.[2,3]

2.2 Waveguide Length

If, for the present, we disregard the optimization requirements for the overall system, then for a given input power and attenuation parameter the choice of a waveguide maximum length is dependent principally on fabrication limitations and on the desire to establish a particular field gradient along the structure. For example, with a constant gradient design[7] the RF power loss per unit length is maintained at a constant value by varying the attenuation along the waveguide. Therefore, for zero beam loading, the power loss per unit length at each end of the structure can be related to the total length and attenuation by $2I_0P_0 = 2I_\ell P_0 \exp(-2\tau) = P_0[1-\exp(-2\tau)]/\ell$ giving $\ell = [1-\exp(-2\tau)]/2I_0$ and $I_0 = I_\ell \exp(-2\tau)$ where I_0 and I_ℓ are the attenuation constants at the input and output, respectively. Thus, in order to maximize the waveguide length for a given value of τ, it is necessary to select the largest permissible input iris diameter ($2a_0$) as represented by a minimum value of I_0. Since the ratio I_0/I_ℓ remains constant for a given value of τ, the above procedure indicates that the output iris diameter ($2a_\ell$) would also tend to a large value. This is not always the most desirable arrangement, however, and under some circumstances the selection of maximum waveguide length may depend on the minimum (output) value of iris diameter that can be permitted within the system. A situation of this nature can occur in the design of a high attenuation waveguide when the associated requirement for a low ratio of I_0/I_ℓ can only be satisfied by a high value of I_ℓ, i.e., the selection of a small output aperture. The interdependence of these relationships is best illustrated by considering actual design parameters and several waveguide examples.

The microwave design data listed in Table 1 were obtained from a series of measurements on cold stack** circuits of different iris diameter (2a). The geometric characteristics of these $2\pi/3$ mode, 2856 MHz cavities (as incorporated in the MIT accelerator design) are shown in Fig. 2. The group velocity values (v_g/c) were computed from a Fourier series representation of the measured dispersion curves, in a manner similar to that described by Robson,[8] and then used in conjunction with measured values to determine the unit length attenuation constants, $I = \pi f/(v_g Q)$. The circuit space harmonics were evaluated from the results of bead perturbation experiments and this enabled r/Q for the fundamental space harmonics to be obtained from the measured values of total r_t/Q.

Although the discussion which follows refers specifically to the waveguide cavity design shown in Fig. 2, the principles are, in general, valid for other traveling wave circuit configurations. Based on the Table 1 data, an arbitrary selection of typical minimum iris diameters, say 2.0, 2.1, and 2.2 cm, allows corresponding I_ℓ values to be defined as 0.307, 0.252, and 0.208 neper per meter, respectively, and this enables the relationship between τ and the waveguide length to be determined. The Fig. 3(a) curves show this relationship for each of the above mentioned output apertures for constant gradient conditions at zero beam loading. The corresponding dependence of the input iris diameter is shown plotted in Fig. 3(b) such that the two sets of graphs can be cross-referenced. As an example, a $2\pi/3$ mode 2856 MHz waveguide 6.50 meters in length with a total attenuation of 0.805 neper and an output iris diameter of 2.00 cm is seen to require an input iris diameter of 3.05 cm. For a constant value of τ, the graphs illustrate the need for larger input and output iris diameters as the waveguide length is increased; conversely, for a given length it can be noted that larger values of τ require reduced iris diameters. For a minimum iris diameter in the range 2.0 to 2.2 cm (this value is usually determined by beam transmission and circuit pass-band considerations) the Fig. 3 curves show that large values of τ favor long waveguides in the 6 to 10 meter range. Increasing the section length, however, eventually results in undesirably large input iris apertures. Although the upper limit for $2a_0$ is not uniquely defined, iris diameters in excess of 3.1 to 3.2 cm exhibit unsatisfactory characteristics such as low shunt impedance (see Table 1) and large transverse phase gradients across the beam-occupied region of the input coupler. This latter effect is of particular concern in single port side-wall coupled cavities (even when off-set techniques are adopted to ensure that the amplitude of the longitudinal electric field is symmetric about the beam axis[9]) and generally requires the adoption of compensating rectangular waveguide feeds and localized steering in order to minimize undesirable transverse momenta contributions and maintain axial alignment of the beam.

In attempting to optimize a high duty waveguide design, the incompatibility of maximizing both the waveguide length and total attenuation can, in most instances, be satisfactorily resolved by first determining a maximum value of τ as based on the capability of the temperature control system to match the phase sensitivity requirements and then selecting an upper limit of $2a_0$ to establish the maximum length. An optimum condition is achieved with this procedure when the value of τ is such that the waveguide length is uniquely defined by input and output iris diameters which correspond to the specified maximum and minimum permissible values for the system. With the type of structure represented by the Fig. 3 curves and for a minimum iris diameter of 2.0 cm, for example, this optimum is closely approached at an attenuation parameter of 0.87 neper and a waveguide length of 7.7 meter.

Strict adherence to the constant gradient condition of the preceding discussion is often avoided in practice since, apart from economic considerations, the use of predetermined cavity dimensions established solely on the basis of power flow in the fundamental mode precludes the adoption of techniques which require local or extended variations of the field gradient. The inclusion of higher order mode phase shifting regions to counteract regenerative beam break-up is typical of this category, as is the avoidance of electric field breakdown due to beam induction in accelerators which combine high current, low τ waveguides with lower conversion efficiency high τ structures.[10,11] In considering long waveguides, accelerator designers have commonly favored the use of a plurality of short length uniform impedance circuits interconnected by matched transition zones. Structures of this type can closely reproduce the advantageous power flow characteristics of a constant gradient design; and in addition to some cost savings in the cavity machining and stacking operation, this technique enables specific higher order mode resonance characteristics to be incorporated in the waveguide to reduce the effects of self-induced beam deflecting fields.[2,3] For the purposes of comparison, a number of $2\pi/3$ mode, long waveguide designs of the varying impedance and gradient type (with the exception of Darmstadt and SLAC) are shown superimposed on the constant gradient curves of Fig. 3(a).

Finally, not to be disregarded in the selection of a maximum waveguide length are important mechanical considerations such as the brazing procedure for the overall assembly, the complexity and cost of an acceptable RF joint (if used), the difficulty of maintaining a satisfactory high vacuum condition throughout the structure under the adverse conditions of high duty operation, and the waveguide handling, tuning and alignment requirements.

2.3 Shunt Impedance and Beam Loading

The benefit of additional energy gain that can be derived from the use of a high shunt impedance circuit will be dependent on the degree of beam loading required for a given application. Since the energy gain of either a constant gradient or uniform impedance traveling wave structure can be expressed as $V = (r\ell P_0)^{1/2} F(\tau) - ir\ell F'(\tau)$, where F and F' are functions of τ only, and i is the peak current, the first term is seen to represent the maximum or unloaded energy and the second term the regulation or beam loading effect. Thus, $(V_0-V)/V_0 = i(r\ell/P_0)^{1/2} F'(\tau)/F(\tau)$, and for a given value of τ the beam loading parameter $i(r\ell/P_0)^{1/2}$ indicates that the decrement in beam energy, normalized to the unloaded energy, increases with total shunt impedance for a given beam current and input RF power. An increase in shunt impedance of approximately 20 percent as obtained, for example, by reducing the number of waveguide cells from 4 to 3, i.e., $\pi/2$ to $2\pi/3$ mode, offers little improvement in beam performance when low values of τ are used for operation under high conversion efficiency and heavy beam loading conditions.[12] For high duty factor service and light beam loading, however, maximum values of shunt impedance are directly beneficial, and a $2\pi/3$ mode approaches the optimum design for a conventional disc loaded waveguide. (The $2\pi/3$ mode values of shunt impedance listed in Table 1 can be increased by 5 to 10 percent if the added complexity of shaping the cavity and reducing the iris thickness can be tolerated.[13]) Two other methods of increasing the shunt impedance can be mentioned briefly; viz., increasing the system frequency and/or using standing wave cavities.

The room temperature scaling laws $r \propto f^{1/2}$ and $Q \propto f^{-1/2}$ could be exploited by constructing, say, 5712 MHz C-band traveling wave structures. Also, by expressing the phase sensitivity as $\Delta\theta/\Delta f \propto \tau f^{-3/2}$, for the same controlled range of waveguide metal temperature, i.e., constant $\Delta f/f$, the phase error would be proportional to $\tau f^{-1/2}$ indicating that at this higher frequency the attenuation parameter could be increased by 40 percent for the same phase shift. These benefits are more apparent than real, however, since in attempting to take advantage of them severe design restrictions can be encountered due to the accompanying scaling laws, $I \propto f^{3/2}$ and $2a \propto f^{-1}$. Design compromises involving these higher attenuation constants and scaled-down iris dimensions tend to favor shorter waveguides; and when the average power requirements of high duty operation are taken into consideration, abnormally high levels of heat dissipation are usually encountered due to the reduced surface area. Under these conditions a highly sophisticated cooling system is required to adequately control the cavity surface temperatures (especially the thin dics), or alternatively, the waveguide dissipation can be reduced by increasing the number of sections, RF feed losses, and system complexity. These are non-trivial tasks in the design and construction of long multi-section machines, and they constitute a distinct disadvantage of the high frequency approach.

The Los Alamos development of side-wall coupled cavities[14] is a notable example of the increased shunt impedance that can be provided by standing wave structures. These cavities demonstrate unit length shunt impedance values which are 40 to 50 percent higher than comparable traveling wave circuits and have unloaded Q values of 15,000 to 20,000 at S-band frequencies. However, for machines which operate under limited pulse length conditions the protracted build-up time of the accelerating fields places a restriction on the narrowest attainable energy spectrum. For example, if the retarded impedance mis-match effects during build-up are disregarded, the growth of the cavity fields can be expressed as $E_t = E_0 [1 - \exp(-\omega t/2Q_L)]$ where E_t is the electric field strength at time t after commencement of RF source excitation or beam perturbation, E_0 is the steady-state value, and Q_L is the loaded Q of the structure which equals half the unloaded Q for a matched circuit. Thus, for a frequency of 2856 MHz and a loaded Q of 8000, build-up times of 4.1 and 6.2 μsec are required for the field levels to attain 1 percent and 0.1 percent, respectively, of the steady-state value. On the other hand, a high attenuation traveling wave circuit operating at the same frequency can provide beam energies within 0.1 percent of the steady-state value after a delay of only 1.8 to 2.2 μsec, including allowance for delayed beam injection and small transients which remain after expiration of one fill time. Since the prime method of obtaining high duty factor performance with linear accelerators of the Saclay and MIT type is by operation with RF pulse lengths within the range of 5 to 15 μsec and at repetition rates of several thousand pulses per second, the above example showing a loss of 3 or 4 μsec as afforded by the use of high Q standing wave

cavities represents a duty factor and/or resolution restriction of substantial proportions. Although various means are available to increase the rate of field growth in standing wave circuits such as the use of adjustable coupling networks and boosted pulses, the added complexity of system components and controls and the loss of operational flexibility (and in some cases maximum beam energy) are discouraging factors.

Returning to the subject of beam loading, a particularly advantageous characteristic of a high duty cycle machine is that despite inherent low field gradients the accelerator will be subject to less beam loading than a conventional low duty, high gradient machine having the same beam energy and power. This is indicated by the beam loading parameter $i(r\ell/P_0)^{1/2}$ which, for a given waveguide design, requires the peak current to be reduced as $P_0^{1/2}$ in order to maintain a fixed degree of beam loading as the peak power level is lowered. However, for a given average current the peak current and peak power vary inversely with duty factor, causing the beam loading derivative to be reduced as the square root of the increase in duty factor. In practice, an even greater reduction of this loading can be obtained by the use of RF generators which combine reduced peak power ratings with increased average power ratings to provide larger duty factors than those obtained by peak power reduction alone. Duty factors 20 to 80 times greater (with peak powers only 5 to 20 times lower) than those normally associated with high gradient machines can be demonstrated in this manner. Consequently, even when using multiple sections per klystron and very long waveguides, the beam loading derivative can be markedly reduced when operating under high duty cycle conditions. While having a distinct influence on the optimization of the overall system, this characteristic also contributes in no small measure to the attainment of low emittance, narrow energy spectra beams (see section 2.5).

2.4 System Optimization

The costly involvement of installing and operating RF transmitters with high average power ratings invariably demands that a carefully considered economic and technical compromise be adopted by trading-off duty factor for beam energy and capital outlay. Clearly, an initial objective is to minimize the number of RF generators and attempt to compensate for the ensuing loss of beam energy by lengthening the accelerator. In general, a reasonable compromise is approached when the savings due to reducing transmitters approximates the cost of additional waveguides, associated vacuum and water cooling systems, real estate and housing facilities. An advantage which becomes evident during this optimization procedure is that the reduced beam loading at high duty results in a much lower value of maximum or unloaded beam energy than a conventional machine of the same average beam power and loaded energy. The Table 2 data illustrate this feature in a comparison between modules of an existing, 0.1 percent beam duty, high gradient machine and a typical high duty factor system. The comparison is made on the basis of the same attenuation parameter (τ = 0.82 neper), average beam current (150 μA) and loaded energy (400 MeV) and shows the interdependence of duty factor, beam loading, accelerator length and RF power taking into account RF losses in the feed system. In considering two sections per klystron, it can be noted that a large increase in accelerator length and total installed average RF power is required for the 4 MW, 1.8 percent duty system, as compared to the conventional machine, but the lower values of peak current (reduced from 150 to 8.4 mA) reveal the marked loading reduction that can be achieved. In comparing the high duty factor four and two section per klystron modules, the reduced RF power and increased accelerator length relationships are indicative of the need for the aforementioned optimization procedure. In some instances a very satisfactory compromise between accelerator capability and initial capital outlay can be established by combining the attributes of both the two and the four section per klystron modules in the same accelerator system. This approach has an added attraction in that the machine can be uprated at a later date, with minimum disruption to the facility, by adding klystrons and retro-fitting a portion of the rectangular waveguide network. Table 2 also lists data for beam duty factors of 4.8 and 5.8 percent as obtained by reducing the klystron peak power. This enables the peak current to be reduced further while maintaining an average current of 150 μA, but the lower peak RF power results in a heavy loss of beam energy and a slight increase in the beam loading derivatives.

2.5 Beam Energy Spectrum

Before outlining the principle design parameters of the MIT and Saclay accelerators, a brief discussion on the problems of attaining narrow energy spectra may be useful in placing several aspects of high duty factor operation into better perspective. The ever-increasing nuclear physics need for beams of higher intensity and resolution has encouraged, in fact has been primarily responsible for, the continual improvement of accelerator performance over the years. The advent of high duty factor systems operating with long pulses, low levels of beam loading, reduced klystron voltages and hard tube modulators, brings with it the possibility of yet a further improvement in beam resolution. Present day design objectives deal with the problems of achieving large fractions of beam current in 1/10 percent energy bins in order that experiments can be conducted meaningfully with resolutions as low as 1/100 to 1/1000 percent.

Apart from alleviating the beam emittance and space charge difficulties normally encountered in the design of injection systems, the lower peak current at high duty factor assists in reducing several of the more serious contributions to beam energy spread. To illustrate three typical examples, namely, the effect on beam energy due to peak current and RF power fluctuations, the transient contribution due to fill-time electrons, and the reactive phase distortion due to non-optimum phasing at entry to the waveguide, a comparison can be made between an existing 0.1 percent beam duty, high gradient design [Adone (Frascati) long sections, refer to Fig. 3] and modules of a high duty factor system (MIT long sections, refer to Fig. 3 and Table 5) for the same average beam current (150 μA) and waveguide filling-time (T_F = 1.2 μsec).

2.5.1 Peak current and RF power and phase variations. With a conventional traveling wave accelerator the percentage change in loaded beam energy ($\Delta V/V$) due to a given percentage variation of either the peak current ($\Delta i/i$) or the input RF power ($\Delta P_0/P_0$) increases as the absolute value of the peak current is

raised. These variations can be related to spectral quality by differentiating the beam energy equation (see section 2.3) to give $\partial V/\partial i = -r\ell F'(\tau)$ and $\partial V/\partial P_0 = (r\ell/P_0)^{1/2} F(\tau)/2$, thus $\Delta V/V = -(\Delta i/i)\,[ir\ell F'(\tau)]/V$ and $\Delta V/V = (\Delta P_0/P_0)(r\ell P_0)^{1/2} F(\tau)/2V$ giving $\Delta V/V = -(\Delta i/i)\,[(V_0/V) - 1]$ and $\Delta V/V = (\Delta P_0/P_0)\, V_0/2V$. The equations show that the change in beam energy $\Delta V/V$, for a given value of $\Delta i/i$ or $\Delta P_0/P_0$, increases as V is reduced by beam loading. For example, at 11 percent loading $\Delta V/V = -(1/8)(\Delta i/i) = (9/16)(\Delta P_0/P_0)$, at 25 percent loading $\Delta V/V = -(1/3)(\Delta i/i) = (2/3)(\Delta P_0/P_0)$, and at maximum conversion efficiency ($V_0 = 2V$), $\Delta V/V = -\Delta i/i = \Delta P_0/P_0$. The relaxation of $\Delta i/i$ and $\Delta P_0/P_0$ tolerances afforded by the reduced beam loading conditions of high duty factor operation is shown in Table 3 for the two above-mentioned systems and a change in beam energy of 0.1 percent. Since in practice it is difficult to achieve peak current stabilization of less than 1 percent during the pulse, these larger values of tolerable $\Delta i/i$ are most advantageous when maximum beam transmission through narrow energy analyzing slits is desired. Because the absolute values of peak current at high duty factor are low, it is necessary to restrict Δi to approximately 100 μA to meet the 0.1 percent $\Delta V/V$ condition listed in Table 3; and this requires the well-stabilized injection of cleanly-defined (chopped) small bunches of optimally-phased electrons. At 100 μA, the tolerable variation in peak current is one to two orders of magnitude above the level normally encountered due to field emission in the vicinity of the first input coupler,[15] however, with increasing duty cycle and field gradient, as can be expected with superconducting machines, this phenomenon could eventually limit the further improvement of spectral quality.

Even though reduced beam loading conditions permit relaxation of the RF power stability tolerances, the demonstration of $\Delta P_0/P_0$ values as low as those indicated in Table 3 requires the klystron voltage (V_K) to have stringent flat-top, droop and ripple, pulse specifications. Under space charge limited conditions ($I \propto V_K^{3/2}$) the klystron beam power will be proportional to $V_K^{5/2}$, and for constant efficiency the RF power will follow the same law. A change in klystron cathode voltage can therefore be related to the corresponding RF power variation and beam energy spread $\Delta P/P = (5/2)(\Delta V_K/V_K)$ and $\Delta V/V = (5V_0/4V)(\Delta V_K/V_K)$. Thus in order to satisfy a 0.1 percent spectral variation, as shown in Table 3, the klystron cathode voltage fluctuations ($\Delta V_K/V_K$) should be less than 0.06 percent for the low duty case and 0.071 and 0.077 percent for the two high duty cycle examples, respectively. Fortunately, these difficult requirements can be relaxed slightly since the stored energy in the accelerator structure prevents the beam from fully responding to those RF power amplitude perturbations which have time constants small in comparison to the waveguide filling-time.

In discussing beam spectra contributions due to klystron voltage variations, it is appropriate to note that the corresponding RF power fluctuations are accompanied by phase shifts which are caused by variations of the electron transit-time between the klystron input and output cavities. The klystron phase shift ($\Delta\phi_K$) over a given trajectory (S) can be obtained by differentiating the equation $\phi_K = 2\pi S/\beta_e\lambda_0$, which relates transit phase angle (ϕ_K) and electron velocity ($\beta_e c$), to give $\partial\phi_K/\partial V_K = (\partial/\partial V_K)\,(2\pi S\gamma(\gamma^2 - 1)^{-1/2}/\lambda_0)$, where the electron energy in rest mass units is $\gamma = 1 + V_K(\text{keV})/511 = (1 - \beta_e^2)^{-1/2}$. This then gives the relativistically corrected phase shift for small fluctuations of V_K as $\Delta\phi_K = -(\Delta V_K/V_K)\,(2\pi S(\gamma - 1)(\gamma^2 - 1)^{-3/2}/\lambda_0)$. As an example, with a free space wavelength of 10.5 cm and a drift length of 35 cm, a $\Delta V_K/V_K$ variation of 0.1 percent produces klystron phase shifts of 0.70 and 0.89 degrees for cathode potentials of 130 and 90 kV, respectively. Since a decrease in cathode potential is accompanied by a reduction of RF power as well as a lag in phase at the accelerator input coupler, it is possible, at least in principle, to arrange for cancellation of the beam energy variations produced by these effects. For example, if the bunch is positioned at a phase angle (δ) immediately behind the crest of the accelerating field such that at the upper limit of klystron cathode voltage ($V_K + \Delta V_K$) the increase in field strength (ΔE) is cancelled by the advance of the wave ($\Delta\phi_K$), and vice versa, then the beam energy condition at each limit of V_K can be equated as $\sin(\delta + \Delta\phi_K)(E + \Delta E) = \sin(\delta - \Delta\phi_K)(E - \Delta E)$ giving $\Delta E/E = -\cot\delta \tan\Delta\phi_K$. In applying this to the above example, for a 0.1 percent change in klystron cathode voltage and a 0.89 degree phase shift, since $\Delta E/E = 5\Delta V_K/V_K$ (at $i = 0$), the value of δ required to compensate for beam energy variation is given as -94.8 degrees, i.e., 4.8 degrees behind the crest (see Fig. 5(a) for the phase angle convention). This example assumes negligible beam loading, and when moderate values of peak current are used, the reactive phase shift and space charge effects must be taken into account. The klystron and accelerator waveguide phase relationships discussed above assume that the interconnecting rectangular waveguide networks operate under phase stable conditions; and it should be noted that the thermal coefficient of phase change of thick wall, S-band, evacuated rectangular waveguide is 0.084 degree/°C/m at 2856 MHz. (The coefficient is due to two cumulative contributions because both the waveguide physical length and the waveguide wavelengths change with temperature, and the resulting phase shift effects are additive.) This indicates that for phase stable operation ($\Delta\phi < \pm 1$ degree) with long interconnecting waveguide runs (20 - 40 m), as commonly required in high duty factor systems, the average metal temperature variation for a given network should be maintained within approximately ± 0.5°C. Since high levels of dissipation are commonly encountered, it is desirable that metal temperature sensors be utilized for closed loop control of the cooling systems and that the waveguides be thermally insulated.

Finally, it should be noted that the problem of minimizing thermally induced long term phase shifts caused by klystron beam interception is especially important in high duty accelerator systems since operation over a wide range of average power can result in large variations of body dissipation. For an operational adjustment of, say, 10 to 1 in average power, and a normal beam interception figure of a few percent, the klystron body average current can vary from approximately 10 to 100 mA. Even though the intercepted electrons have low energies, average currents of this magnitude can cause the body dissipation to vary from approximately 200 to 2000 watts; and in order to achieve phase stability under these conditions, an effective cooling system for the RF cavity and drift tube assemblies is an essential prerequisite.

2.5.2 Transient contributions due to fill-time electrons. Since the filling-time is constant for a given waveguide, the contribution to energy spread due to transients becomes less important as the beam pulse length is increased. Also, for high duty factor systems with long pulse capability, there is usually little concern regarding a small loss of beam pulse length, and full advantage can be taken of minimizing the transient by delaying the injected current with respect to commencement of the RF pulse. The spectral improvement gained from this procedure depends on the degree of beam loading as illustrated in Fig. 4. This figure compares the transient beam loading characteristics of the 0.1 and 1.8 percent duty systems listed in Table 3 for a range of beam delay times (t_{bd}) extending from zero up to one fill-time (T_F). In Fig. 4(a), the large transient energy spread associated with the heavier loaded system is reduced to a total bin of approximately 14 percent with a beam injection delay of 0.5 T_F whereas a beam delay of 0.8 T_F for the high duty example of Fig. 4(b) limits the total $\Delta V/V$ to 7 percent. Although energy spreads of this magnitude result in a foreshortening of the analyzed pulse and are too large for most experimental purposes, an improvement in the overall performance of multisection machines can be demonstrated with this technique by programming the RF transmitter triggers to provide partial cancellation of the transients.[16]

2.5.3 Reactive phase distortion and bunch width. If a small bunch of relativistic electrons is phase displaced slightly from the peak position of the accelerating field at entry to a correctly tuned waveguide operating with a phase velocity equal to c, then interaction between the applied and beam-induced electric fields will result in a beam loading phase shift between the total RF field and the bunch. Regardless of whether the entry phase is behind or ahead of the crest, the initial phase difference will increase continually with distance along the structure at a rate dependent on the peak current, applied field and phase position of the bunch centroid at entry to the waveguide. This increasing phase displacement occurs because the in-phase component of the circuit field is reduced by both beam loading and copper losses whilst the quadrature component is attenuated by only wall losses. The effect is shown vectorially in Fig. 5(a) for the indicated phase convention of $\delta = -\pi/2$ at the peak of the accelerating field. For an initial phase angle $\delta_0 \neq -\pi/2$ and a total electric field E_0, at a given distance along the waveguide the in-phase component of field E_1 is reduced to E_1' by the normal copper losses and by the growing beam-induced field E_b'. On the other hand, the quadrature component E_2 is reduced to E_2' by the copper losses only. Thus the original total field vector rotates further away from the in-phase vector and is reduced to E' in accordance with the dissimilar reductions of E_1 and E_2. The rotation of the total field vector to a new phase position represents a reactive phase shift or distortion of the circuit wave due to the presence of charge in the structure. For resonant frequency operation under correctly tuned conditions, the beam loading phase shift is such that when the centroid of the bunch is located at $-\pi/2 < \delta < \pi/2$, the wave will slip back with respect to the bunch, and when located at $\delta < -\pi/2$ or $\delta > \pi/2$, the wave will advance with respect to the electron bunch.

For a constant impedance waveguide the emergent phase angle δ can be related to the entry phase δ_0 by the expression

$$\tan \delta = \tan \delta_0 + ir(\exp \tau - 1)/(E_0 \cos \delta_0)$$

where E_0 is the amplitude of the fundamental component of longitudinal electric field at entry to the waveguide. In the case of a constant gradient design (at i = 0), the above relationship can be expressed as

$$\tan \delta = \tan \delta_0 + ir\tau/(E_0 \cos \delta_0) .$$

The reactive phase shift dependence on entry phase angle and beam loading is shown in the Fig. 5(b) graphs of entry phase versus emergent phase for the two waveguide designs compared in Table 3. The previously used peak current value of 8.4 mA for the high duty factor example (to match the 150 μA average current of the 0.1 percent duty system) has been increased to 25 mA in this comparison so that extreme examples of phase shift and energy spread can be considered. For the low duty factor system, operating at an input RF power of 9.8 MW and a peak current of 150 mA, entry phase displacements from crest of 2 and 5 degrees result in emergent phase displacements of 7 and 17 degrees, respectively. With the high duty factor system operating at 1.8 MW input RF power and a peak current value of 25 mA, similar initial phase displacements of 2 and 5 degrees cause emergent displacements from crest of only 3 and 7.5 degrees, respectively. When operating at a given average beam current, the reduced reactive distortion of the lighter loaded machine indicates that beam spectrum contributions due to system phasing discrepancies will be lower for the higher duty factor accelerator.

Since the beam energy spread due to reactive distortion grows rapidly with small increasing initial phase displacements, it is necessary that phase drifts during the pulse be reduced to an absolute minimum in order to achieve high resolution performance. In this regard, attention must be directed at limiting the klystron cathode voltage droop (especially if long pulse operation is necessary) and avoiding the introduction of phase drifts from the klystron driver. Some reduction in beam energy spread due to klystron voltage droop can be obtained by phasing the bunch behind the crest since not only does the phase lag tend to compensate the loss in gradient (see section 2.5.1) but the forward migration of the bunch, due to the drooping pulse, tends to oppose the reactive phase shift. However, even a small phase overshoot of the bunch ahead of the crest at entry to the waveguide will result in subsequent phase slippage and energy spread due to reactive distortion. The beam energy spread $\Delta V/V$ due to small entry phase shifts is shown in Fig. 6 for the 1.8 percent duty example of Fig. 5(b) and a range of input RF peak power levels from 1.8 to 0.2 MW. These curves take reactive phase shift effects into account and apply to particles located at the centroid of the bunch (for i = 25 mA) whereas the comparative graph for the unloaded condition refers to single particle energies and therefore reactive distortion effects are not considered. The total energy spread due to all particles in a relativistic bunch of width $\Delta\delta$, centered about the crest, can be determined from the small angle approximation $\Delta V/V = 1 - \cos(\Delta\delta/2) \approx -(\Delta\delta)^2/8$. At zero beam loading, therefore, the 0.1 percent $\Delta V/V$ produced by an on-crest 5 degree bunch will increase by $[2(2.5 + 2)]^2/5^2$ to 0.31 percent for a 2 degree phase drift during the pulse, whereas a 2 degree bunch subject to the same phase drift will cause $\Delta V/V$ to increase from 0.02 to 0.14 percent. These

results can be obtained directly from the zero beam loading curve of Fig. 6 by selecting a δ_0 displacement from the crest which equals the phase drift plus half the bunch width. Since the $\Delta V/V$ values for the beam loaded examples refer to particles located at the centroid of the bunch (obtained by integrating the changing field amplitude, due to copper loss and reactive phase shift, during traversal of the structure), the contributions due to the finite width of the bunch must be added, as before, to obtain the total $\Delta V/V$.

In realizing the practical difficulties of limiting phase drifts during the pulse to less than 1 or 2 degrees and taking the above effects into account, it is apparent that the demonstration of large fractions of current within $\pm$ 0.1 percent of $\Delta V/V$ requires that the bunch be confined within a very narrow region of longitudinal phase space, preferably less than 2 degrees.

2.5.4 Space charge longitudinal fields and low gradient operation. With a low gradient, high energy resolution accelerator, the longitudinal space charge fields generated by small bunches of electrons can contribute significantly to the beam energy spread, even when relatively low values of peak current are used, if the bunch is phased at or near the crest of the wave before a sufficiently high beam energy is attained. Ideally, the electron energy spread will be reduced to a minimum when the centroid of the bunch is located ahead of crest at a phase position such that, for a given accelerating field strength, the applied gradient over the length of the bunch is always sufficient to counteract the longitudinal field gradient due to space charge. In considering electron energies greater than 10 MeV, de-bunching effects can be neglected, and evaluation of the space charge fields enable the centroid phase position to be determined from a knowledge of the circuit field strength and bunch length. In practice, non-uniform charge density distributions and irregular bunch geometry lead to asymmetric and non-linear space charge field distributions within the bunch. A reasonable approximation can be obtained, however, by assuming a spheroidal bunch model of uniform charge density. Then, for a small bunch, $\Delta\delta^o$ long, the space charge field gradient will be counteracted by the applied gradient when $E_{sc} = E_z \cos \delta_m \sin(\Delta\delta/2)$, where δ_m is the phase position of the bunch centroid, and E_{sc} and E_z are the terminal space charge and circuit field strengths, respectively. This relationship provides an indication of the allowable proximity of the bunch to the crest for maintaining a minimum energy spread condition. As an example, the Fig. 7 curves show the nearest centroid phase position (δ_m) that can be permitted for beam energy values up to 100 MeV, and a typical high duty operational field strength of only 20 kV/cm. The space charge calculations were based on a spheroidal bunch model of uniform charge density containing 5.5×10^7 electrons (25 mA at 2.856 GHz). An interesting conclusion drawn from these curves is that low field gradient operation with small bunches and moderate beam loading requires ahead-of-crest phase location over a considerable length of the machine if space charge energy spread contributions are to be avoided. The degree of relaxation afforded by increasing the bunch diameter or reducing the peak current is also shown in Fig. 7 for the 2 degree bunch example. A space charge requirement that the bunch be located ahead of the crest, when traversing the waveguide sections at the beginning of the machine, is contrary to the requirement for pulse droop and reactive phase shift compensation, and emphasizes the need for a comprehensive means of analyzing the spectral influence of these various effects.

3. Principal Design Parameters

The design characteristics of the Saclay and MIT accelerators are listed in Tables 4 and 5, respectively. Hard tube modulators were chosen in both systems as the method most likely to demonstrate reliably the high quality specifications and also because of the need for high repetition rates. The systems differ, however, in that the Saclay modulator design makes use of a pulse transformer and two switch tubes to provide high voltage pulses for the klystron cathode while the MIT transmitter design utilizes two paralleled switch tubes in series connection with each klystron for direct high voltage switching. These series switch tubes are gridless and utilize magnetron injection gun geometry with the cathode well protected from arcs. A high plate resistance is an essential characteristic since it provides the regulation necessary for meeting the jitter and drift specifications and allows economy in the energy storage capacitor banks. The plate resistance of the two switch tubes in parallel is more than twenty times the dynamic impedance of the klystron. The relative merits and technical details of the two different transmitter systems have been discussed elsewhere,[2,3] and additional information is shown in Tables 4 and 5. The capability of continuously varying the peak RF power and pulse length over the entire dynamic range of the system is an important feature of the direct series switching approach. With a given maximum rating of average RF power, the selection of a peak RF power operating level automatically defines the maximum permissable duty factor, and this can be achieved with many combinations of pulse length and pulse repetition rate. For example, the broken curve in Fig. 8 depicts the inter-relation between maximum RF duty factor and peak RF power for the MIT transmitter design; and the full curves compare the limiting values of peak RF power and repetition rate for different values of RF pulse length.

The following sections contain brief descriptions of the RF system and beam centerline components of the MIT accelerator, further illustrating some of the design problems common to high duty factor machines.

4. RF System

The microwave distribution system and arrangement of accelerator waveguides for the MIT project are shown schematically in Fig. 9. At high duty factor, the provision of a reliable, phase stable RF drive system extending over the full length of the accelerator presents a severe design problem owing to the high levels of power dissipation. One method of avoiding this problem, and thereby enabling the desirable features of a coaxial line to be retained, is shown in Fig. 9. (Since v_g can be closely approximated to c, and because of low dispersion characteristics, a coaxial line is more tolerant to small changes of frequency and temperature than a rectangular waveguide, and is advantageous for electron beam phasing purposes.) Drive power for the main klystrons is obtained from intermediate klystrons which are excited via a common coaxial line from a master RF driver. While this technique offers several distince advantages, especially the very low power rating permitted for many of the components, extreme care must be taken to avoid radiative feedback into what is

essentially a long distributed 100 dB cascaded amplifier system. A potential source of interference is the RF leakage associated with isolated collector high power klystrons; and low-level drive line components such as couplers, flanges, etc. should be well shielded and/or remotely located in a shielded duct.

The RF master exciter consists of a tunable phase-locked crystal-controlled solid state oscillator which drives a water-cooled klystron. All phase-lock and oscillator components are oven controlled for high stability, and pin-diode modulation capability of the oscillator output (400 mW) enables optional cw or pulsed operation of the klystron. The klystron is rated at 1 kW cw, requires a drive of 200 mW and is energized by a remotely adjustable 8 kV regulated dc power supply having a ripple voltage specification of less than 0.01 percent peak to peak. Power from the main 1-5/8 inch coaxial drive line is coupled out at five locations along the machine (via adjustable attenuators) to excite a series of 1 kW klystrons, each of which provides drive for two high power klystrons. With this approach, even at 10 percent duty, the total dissipation in the main drive line is limited to less than 70 watts, and the drop-out lines (2 W peak) and components connecting to the driver klystrons operate at an average power of a few hundred milliwatts. The five driver klystrons are identical in design to the master driver klystron and are similarly energized from highly stabilized dc power supplies. Thus, all driver klystrons operate with dc beams and derive pulsed input RF signals from a trigger-logic-controlled modulation of the master oscillator output. This drive system concept was chosen as the most likely to reliably provide a 1 degree phase stability for the main klystron drive signals as well as for the main drive line in its role as a master reference for phasing the accelerator. (The master oscillator provides a cw low level signal which is also available for this purpose.) The support and stabilization of long coaxial drive lines have been discussed elsewhere,[17] and it is sufficient to note here that the 180 meter MIT main drive line requires an ambient temperature control within $\pm$ 0.5°C and a gas (dry N_2) pressure stabilization of less than $\pm$ 0.1 psi.

The high power klystrons are of 5 cavity construction, requiring a peak RF drive of approximately 50 watts, and a single output feed is used with the waveguide terminated in a half wavelength (solid block) water-cooled ceramic window. A short section of thick-wall, pressurized waveguide, terminated with a similar RF window, connects the klystron to the evacuated rectangular waveguide system. This section serves the dual role of providing additional cooling for the klystron window (average power 80 kW) and enabling klystron replacement without disturbing the vacuum system. It also provides a convenient location for the four directional couplers used for RF protection and monitoring purposes. The evacuated rectangular waveguide networks are similar to those used at SLAC, with the exception that an extra water cooling channel has been added to the high power sections between the klystrons and the power splitters. Metal temperature sensors are provided on various branches of the network to limit phase excursions during operation by automatically controlling the inlet water temperatures. RF monitoring couplers are located on either side of the driver and main klystrons and in the rectangular waveguide feeds immediately prior to each accelerator waveguide input coupler. In order to minimize transverse momenta contributions to the beam, due to coupler asymmetries, the rectangular waveguides are arranged as vertical input feeds from above (A) and below (B) the 22 accelerator structures in an ABBA BAAB ABBA BAAB BA BAAB configuration, as shown in Fig. 9. To further cancel the effects of coupler asymmetry, the input and output RF feeds are located on the same side of each accelerator waveguide; and, to provide local correction, two pairs of beam steering Helmholtz coils are located at each input coupler. In keeping with a philosophy to avoid unnecessary evolution of gas within the vacuum system, especially during long pulse operation, the accelerator waveguide output feeds are connected to water loads which are isolated from the vacuum by two quarter wavelength ceramic windows separated by a short section of air-filled rectangular waveguide. Again, this section serves the dual purpose of providing a convenient location for the output RF power monitor and avoiding a catastrophic situation in the event of a window failure. Since there are no high power phase shifters in the system, reliance is placed on the accurate determination and manufacture of the rectangular waveguide lengths and on final tuning of the waveguides after installation to provide correct phase relationships within individual networks.[18] A set of coaxial cables running alongside the temperature controlled main drive line will enable RF signals from the various monitoring couplers to be conveyed directly into the control room by remote operation of coaxial switch combinations.

5. Accelerator Waveguides

Two series-connected accelerator waveguides, comprising a portion of the injector, are followed by four short (3.7 m) and eighteen long (7.4 m) waveguide sections. The klystron interconnections and the waveguide layout are shown in Fig. 9, and the waveguide details and beam specifications are listed in Table 5. The first klystron is reserved for the injector, and the second and third klystrons excite two short sections each to provide a maximum gradient of 50 kV/cm (at an RF duty factor of 2 percent) at the beginning of the machine. The long waveguides are connected such that five klystrons service ten sections and two klystrons the last eight sections. The waveguide sections are divided into various groups (designated AA through D, see Fig. 9) which are similar in mechanical design but differ in microwave characteristics, as described below. With the exception of the injector buncher section, each waveguide contains eleven uniform, $2\pi/3$ mode segments of increasing impedance, interconnected by transition regions.

Each long waveguide uses 100 gpm of de-mineralized water passing in reverse direction through a uniflow configuration of eight, full-length, 16 mm inner diameter cooling tubes which are silver brazed to the outer wall of the waveguide. A flow of 100 gpm and a uniflow cooling design were also chosen for the 3.7 m waveguides; but in order to obtain a comparable performance with the higher loss per unit length of these short sections, twelve, 11 mm inner diameter, full length tubes were specified, i.e., a water velocity of 555 cm/sec. Metal temperature sensors are located at unique positions on the waveguides to provide phase shift correction for a wide range of beam loading and average RF power settings by automatically controlling the inlet water temperature.[3] The longitudinal location of the temperature sensing bulb depends on the particular

waveguide design and on the direction of water flow along the section. Each short waveguide is connected for forward flow and has a sensor located 2.3 meters from the input coupler. For the long sections and reverse water flow, the distance of the sensor from the input coupler varies from 5.15 meters for the first group of waveguides (A) to 3.1 meters for the last group (D). The effective azimuthal location of the sensor bulb is approximately 10 degrees from the centerline of a cooling tube, and the brazed sensor assembly is provided with a thermal radiation shield. Each accelerator waveguide is housed in a separate stainless steel vacuum jacket[19] having an inner diameter of 16.5 cm, and individual cavities are provided with eight pump-out holes, as shown in Fig. 2.

5.1 Beam Breakup Considerations and Microwave Design Details

The cumulative type of beam breakup experienced and subsequently identified at SLAC[20] is of particular interest to the designers of high duty factor linear accelerators because the low gradient, long pulse operational requirements are conducive to this phenomonen and could result in a serious limitation of peak current. For example, the MIT machine specification of 60 kW of beam power at 400 MeV and 1.8 percent duty requires the demonstration of a peak current of 8.4 mA over a range of pulse lengths up to 14 μsec; and an extrapolation based on SLAC experience, under conditions of weak focusing, suggested that a cumulative beam breakup threshold value of between 5 and 10 mA could be expected. As a consequence, several microwave design approaches were investigated with the aim of elevating the threshold value to a safe level. A design value of 50 mA was chosen as a goal since the low gradient waveguides at the end of the machine (four sections per klystron) have an i_m value of 60 mA when the klystron is operated at the specified maximum RF peak power of 4 MW. Since, for a given accelerating gradient and charge per pulse, the cumulative type of beam breakup is strongly dependent on the number of identical resonant elements which can interact with the beam and on the HEM_{11} transverse shunt impedance,[21,22] the investigations were concentrated on means of reducing the coherency lengths, and on HEM_{11} Q-spoiling techniques. In regard to the former, an obvious approach is the interspersion of waveguides with different HEM_{11} resonant characteristics along the machine; and this technique was adopted for both the Saclay and MIT projects. With these machines, a constant $2\pi/3$ phase shift per cavity in the TM_{01} mode was maintained, and the HEM_{11} resonant values were varied by suitable selection of the iris aperture dimension (2a) and the cavity diameter (2b). Typical HEM_{11} mode dispersion data for a range of 2a values, as obtained from cavity cold stack measurements (see Fig. 2 and Table 1 for cavity details), are shown in Fig. 10.

With the MIT design, although consideration was given to HEM_{11} resonances in each of the distributed uniform impedance segments, in view of the SLAC experience, more importance was placed on beam interactions in the first few segments of the waveguides and on resonances in the vicinity of the $v_p = c$ intercept (which occur near the HEM_{11} π mode for TM_{01} $2\pi/3$ mode structures). It was expected that HEM_{11} resonances generated in segments remote from the input coupler would be less troublesome because reflections between the input coupler and the edge of the HEM_{11} stop band for a given segment are subject to higher attenuation the further the segment is along the structure, and because the group velocities are, in general, quite low. Moreover, as the reflection path lengths increase, the interaction effective lengths are curtailed due to large (multiple π) phase slips between the wave and the beam. In this regard, it is important to avoid excessive reflections of the backward propagating wave within the body of the waveguide by using matched transitions and disc apertures which increase in diameter towards the input coupler, and, whenever practicable, to avoid increasing the interaction by preventing resonances in a given segment from coinciding with resonances at a lower βD in a preceding segment nearer to the input coupler. In considering the dispersion curve for a given uniform impedance segment, strong beam interactions can be expected in the proximity of the $v_p = c$ intercept, especially for large iris diameter segments which are longer than three wavelengths, because the resonances are closely spaced in this region (see Fig. 10), i.e., the $d\omega/d\beta$ values are very low. Under these conditions, the beam interaction can more readily establish the worst value of total phase slip which satisfies the condition for maximum transfer of energy to the fields and beam deflection amplification.

5.1.1 Progressive stop-band technique applicable to initial segments of the waveguide. The design of the waveguides for the MIT accelerator was strongly influenced by the adoption of a progressive stop-band concept which required a specific relationship between different waveguide sections along the beam centerline. In this accelerator, the eighteen long waveguides are divided into four groups, each of which are similar in physical detail but differ in microwave design. The groups are designated A through D, and the layout arrangement is indicated in Fig. 9. The HEM_{11} dispersion characteristics for the group A waveguides are arranged so that the narrow bands of closely spaced undesirable resonances associated with the input coupler and several of the adjoining uniform impedance segments, in the vicinity of the $v_p = c$ intercept, are displaced outside and below the HEM_{11} pass bands of all subsequently located structures, regardless of group affiliation. Similarly, the range of HEM_{11} resonances associated with the critical initial regions of the group B waveguides are designed to fall below the HEM_{11} pass band regions of all following waveguides in groups C and D. This stop-band procedure is applied progressively along the full length of the accelerator. In this manner, the displacement modulation information carried by the beam at low HEM_{11} frequencies, due to transverse fields in the initial segments of waveguides in an upstream group, is excluded from interacting with downstream waveguides; and further deflection amplification at these frequencies is avoided. When using disc loaded waveguides of conventional construction, this technique requires that the iris diameters in the initial region of waveguides in a given group be smaller than those in any preceding group but larger than those in subsequently located groups.

The above progressive stop-band concept is illustrated diagrammatically in Fig. 11. Curves A_1, B_1, C_1, and D_1 represent the HEM_{11} ω-β diagrams for the input coupler and the first uniform impedance segment of the waveguides in groups A, B, C and D, respectively. Similarly, the dashed curves A_2 through D_2 and A_3 through D_3 refer to the second and third uniform impedance segments, respectively. These curves also show some of the low value HEM_{11} resonances as determined

by the number of cavities per segment, the input coupler phase shift, and the phase shift in the terminating transition in which pass-band cut-off occurs. (A series of cold test experiments were conducted using different transition designs and offset input couplers to measure the terminal phase shift values and HEM_{11} field patterns for both orthogonal planes of polarization.) For the input segments of waveguides in a given group, the Fig. 11 curves show that undesirable resonances in the proximity of the $v_p = c$ intercept are located below cut-off for the pass band of any following group and that these resonances are separated by approximately 30 MHz from those of corresponding segments in the waveguides of neighboring groups. Separations of this magnitude ensure that a frequency coincidence with any following group is restricted to a low value of βD, e.g., 90^o instead of 165^o; and therefore, less troublesome wave-beam phase slips of large magnitude can be expected (90^o to 45^o per cavity).

5.1.2 Other microwave techniques, interactions, and design data. It should be noted that other methods exist for varying the waveguide HEM_{11} resonant characteristics, in order to avoid coherent interaction along the beam centerline, and that changes in iris aperture and/or TM_{01} phase shift per cavity are not always necessary. For example, the number of cavities per segment can be altered and/or small grooves can be machined in the iris to vary the HEM_{11} phase shift without unduly affecting the principle mode. While these methods are limited in scope, both, particularly the former, have obvious advantages since the same disc and cylinder components can be machined for many waveguides, and several groups of different design can be formed by retaining the transition combinations and simply changing the segment lengths. This technique was used in the design of the four short waveguides for the MIT accelerator. These sections are divided into two groups (designated AA and BB as shown in Fig. 9), the waveguides of which have different HEM_{11} resonances although they are constructed from identical components. As before, the input coupler region was of the greatest concern; and by arranging a variation of approximately two to one for the first segment length, a separation of approximately 5 MHz was obtained over the region $\pi/2 < \beta D < \pi$ for all but one pair of resonances. This pair consisted of the first (dominant) HEM_{11} resonance in the AA group and the second resonance in the BB group. However, the downstream resonance results in a low value of total transverse shunt impedance because the wave-beam phase slip through the segment closely approximates 2π. By maintaining the same number of uniform impedance segments for all waveguides, the interaction effective length at the dominant HEM_{11} frequency is, in general, much less for segments in the short, lower energy waveguides. There is a further tendency for the total transverse shunt impedance to be reduced due to a higher value of α and a lower transit time factor $[T = (\sin \alpha/2)/(\alpha/2)]$ normally associated with a short segment resonance. The total phase slip of the wave relative to the beam ($\alpha = n\delta + \epsilon$, where n is the number of uniform cavities per segment, δ the wave-beam phase slip per cavity and ϵ the terminal phase shift correction) tends to increase as the circuit length (nD) is reduced, e.g., with a $5 - 6\,\lambda_0$ (TM_{01} $2\pi/3$) segment, $\alpha \approx 30 - 40^o$ compared to $\approx 120^o$ for a $2 - 3\,\lambda_0$ segment (2a = 1.1"); and the effective length is reduced accordingly ($L_{eff} \propto T^2\,nD$).

When waveguides of different design are interlaced along the machine to reduce the deflection amplification caused by cumulative beam breakup, various interactions need to be considered. These include interactions which occur between segments of the same waveguide, between waveguides of the same group, and between waveguides of different groups. In addition, whenever possible, the design should be arranged to prevent the occurrence of beat frequencies[23] within critical frequency bands. Since the HEM_{11} frequency is approximately 2/3 that of the fundamental accelerating mode, a beat with the third harmonic of the bunched beam (8568 MHz) is of particular concern because the HEM_{11} resonance and its difference frequency can be in close proximity (overlap occurs at 2a = 0.850"), and the advantage of the progressive stop band feature can be nullified. For the MIT long waveguides, the computed dominant HEM_{11} resonances for groups A through D are 3948, 3980, 4010 and 4040 MHz, respectively, and these result in third harmonic difference frequencies (between 4620 and 4558 MHz) which are well removed from the critical stop-band regions. Another aspect which is of some concern, especially at the beginning of low gradient machines, is the possibility of establishing a HEM_{11} wave-beam phase slip of approximately π, in one of the low energy waveguide segments, at a frequency which can excite subsequently located cavities. Due to feedback, this phase slip condition can result in an oscillatory beam deflection (regenerative beam breakup mechanism), and even though this deflection is small in magnitude (e.g., $\approx 10^{-4}$ cm), because of its coherent nature, through subsequent interaction, it can cause the cumulative beam breakup threshold current to be substantially reduced.

Design data for the MIT machine and computed HEM_{11} frequencies (dominant and up to the fourth resonance) relating to the first three of the eleven segments for each waveguide group are listed in Table 6. Initial calculations of the deflection amplification, due to cumulative beam breakup, for peak current pulses in the range of 10 μsec ($T \gg 2Q/\omega$) and Q values of 9000, indicated that, for changes in waveguide design and grouping as described above, a reduction of approximately 6 e-folding factors could be expected. (At 4 MW peak RF power per klystron this represents a threshold value in excess of 40 mA at 10 μsec.)

Computer calculations also indicated that beam displacements, for example, those due to section misalignments of the order of $\pm\, 5 \times 10^{-2}$ cm, could increase the beam deflections to a critical level during the transient growth of the cumulative beam breakup mode. The computed deflections reached maximum levels approximately 3 μsec after commencement of the beam pulse and thereafter attenuated to steady-state asymptotic values. These results justified further an existing philosophy which placed emphasis on producing a low emittance beam from the injector and on accurately positioning the beam along the axis of the machine. (Steering coil assemblies are provided at every input coupler, and the waveguide construction and installation procedures call for axial alignment to beter than $\pm\, 3 \times 10^{-2}$ cm.)

The above results suggested that additional precautionary measures, such as the provision of special Q-spoiling circuits, were unnecessary. A worthwhile

reduction of Q is achieved in a relatively simple manner, however, by deforming the cavities in a specific orientation during the normal tuning procedure. With this technique, originally used on very short section, high current, long pulse machines,[24] an attempt is made to improve the match of the terminating cavities by coupling the HEM_{11} mode into the external system. Individual cavities are tuned (permanently deformed) in a radial plane at $\pm 45^{o}$ to the plane of the rectangular waveguide feed; and for a given set of cavities, the deformation is applied in only one plane, i.e., the cavities of a given segment contain only two wall perturbations, and these are diammetrically opposed. In this manner, partial coupling can be obtained for either of the orthogonal planes of polarization, and loaded Q values approximately 30 percent less than Q_0 ($\approx$ 10,000 at 4000 MHz) can be obtained.

In summarizing, it can be noted that the technique of mixing different waveguides becomes more difficult as the length of the machine is increased. The need to adjust iris diameters to vary the HEM_{11} characteristics interacts strongly with, and causes modification of, the fundamental accelerating mode design requirements such as τ, ℓ, field gradient distribution, offset couplers, etc., until eventually the limiting values of resonance separation and/or iris diameter are reached. Also, the design procedure can be affected by economic considerations which impose restrictions on the number of different waveguide components that can be made available. As an example, the MIT long waveguides were designed for constant τ with progressively smaller input iris apertures but with the restriction that all output couplers were to be of the same design. Although not the most desirable from an operational point of view, beam focusing methods have been shown[21,22] to offer a practical and economic solution to the problem of raising the cumulative beam breakup threshold current; and in considering future high duty cycle machines of long length, the best economic compromise may well be a combination of both microwave and focusing remedies.

6. Injection System

As with conventional machines, the injector plays a key role in the ultimate performance of a high duty factor accelerator, particularly in regard to minimizing longitudinal phase space and beam emittance. However, the wide range of input RF power, unique to a high duty system, presents a problem in the design of the first waveguide and other injector microwave structures which are used for processing and positioning the electron bunches. One method of overcoming this problem is to arrange for a separate modulator and klystron to always energize the injector at a low level of peak RF power. In this manner, the full range of beam duty can always be provided by the injector, regardless of the level of peak and average RF power required by the remainder of the machine. Because the field gradient associated with this technique is low, adequate capture and bunching of injected electrons usually necessitates the use of a reduced phase velocity waveguide, and, careful account must be taken of the space charge forces if undesirable limitations to bunch width are to be avoided. This is especially the case during operation at low duty factor when all klystrons, with exception of the injector, are at maximum peak power, and there is a demand for high values of peak current. With a tapered phase velocity structure, the bunch tends to maintain a constant energy by automatically adjusting its position on the wave, and the emergent phase is therefore a sensitive function of input power level and,to a lesser degree, beam loading. An operational advantage of the fixed low power level concept is that the drive for the injector drift space cavities remains unaltered.

An alternate design approach, as chosen for the MIT injector, is to operate at high gradient up to a duty factor of 1.8 percent, which is the condition requiring maximum peak current values, and to allow the buncher waveguide gradient to be reduced for operation at higher duty factors. Although this technique requires an adjustment in phase between the injector and the remainder of the machine when a different level of peak RF power is selected, it provides the maximum beam energy gain for a given combination of modulator and waveguide; and, with a suitable gun voltage, full advantage can be taken of the bunch compression properties of a velocity of light waveguide.

Consistent with the inherent high resolution of a lightly loaded accelerator, the MIT injector design studies placed emphasis on means of attaining narrow bunch widths. The design objectives were based on a specification of two degrees of longitudinal phase space at not less than 6 MeV and 25 mA with a peak RF input power of 2.5 MW. Emphasis was also placed on minimizing the cost and number of components while keeping in mind the high stability requirements of the system. The concept chosen as most likely to meet these objectives was based upon the use of a low perveance ($\approx 10^{-9}$), high voltage source and two stages of bunch compression. The first stage is designed to operate at beam energies within the range of 300 to 500 keV and to provide a bunch compression of between 15 to 1 and 20 to 1 with the approximate sawtooth field environment of a 120 degree biased-chopper prebuncher combination. At these values of beam perveance and energy, a relatively low drive signal at the prebuncher can cause the longitudinal space charge fields to be dominated during bunch compression down to very small dimensions. The second compression stage consists of a disc-loaded waveguide designed to provide approximately 5 to 1 compression of the bunch during initial retardation and acceleration from 0.3 to 7 MeV. Apart from the input coupler and several neighboring cavities, which have phase velocities slightly less than c, the structure is designed as a $2\pi/3$ mode, $v_p = c$ circuit. The high gun potential, small cathode, and long focal length, in combination with a narrow collimating aperture and a low value of longitudinal phase space at injection to the buncher, hold promise of demonstrating a considerably lower beam emittance than that normally obtained from higher perveance injection systems. Some of the considerations and results of analyses which led to this concept are discussed in the sections which follow.

6.1 A Pessimistic Conclusion Regarding Permissible Injection Velocity Spread for a $v_p = c$ Waveguide

Some guidance regarding the tolerable limits of phase spread and velocity modulation at injection, to achieve a given narrow emergent phase spread with a $v_p = c$ waveguide, can be obtained from the binding field expression[25]

$$\cos \delta_a = \cos \delta_0 - \left[(1-\beta_0)/(1+\beta_0)\right]^{1/2} 2\pi m_0 c^2/(eE_0 \lambda_0)$$

where δ_0 and δ_a are the input and asymptotic phase positions, respectively, for a single particle of velocity $\beta_0 c$ injected into a $v_p = c$ waveguide having a longitudinal electric field fundamental space harmonic amplitude of E_0. With an injection phase angle corresponding to the zero field position ($\delta_0 = 0$) and an asymptotic phase spread of either one degree or two degrees, this equation indicates that the permissible spread of energy (ΔV_0) and velocity ($\Delta\beta_0$) at injection must be limited as shown in Table 7. For example, to obtain one degree asymptotic phase spreads when using injection energies of 100, 200 or 400 keV, the energy and velocity spreads at injection must be limited to 6.0, 8.8, and 13.4 keV and 1,22, 0.9 and 0.55 percent of c, respectively. It should be noted that these values are obtained from a simple binding field theory which does not include the effects of cavity space harmonics, entry fringe field or the presence of charge.

It has been shown,[26] for $2\pi/3$ waveguide, that space harmonics cause broadening of both the bunch and the energy spectrum and, for a phase velocity of light circuit, this broadening increases as the injection energy is reduced. It has also been shown that if bunches are to be located ultimately at the crest of the traveling wave, then entry into the coupler cavity has to occur during a decelerating phase which causes the injected bunch to be first retarded and then accelerated prior to arrival at the mid-plane of the cavity. This interaction takes place in a field environment similar to that of a standing wave, i.e., in the presence of two equal opposing space harmonics; and the full complement of space harmonics constituting the main traveling wave is not encountered until further penetration into the circuit has occurred. Injection analyses using $v_p = c$ accelerator waveguides and taking into account the different spatial harmonic content of the input coupler, as well as the entry fringe field effect, indicate that for a given emergent phase spread, the tolerable values of energy spread at injection are considerably lower than those given by the above binding field formula. Some of these lower values, as modified by space harmonic analyses, are shown in brackets in Table 7. The modified values of permissible injection energy spread decrease with reduced gun potential, as before, but in accordance with a must narrower range of permissible velocity modulation. A comparison of the tolerable ΔV_0 and $\Delta\beta_0$ values for a fixed injection phase angle and a range of gun potentials, to give a one degree emergent phase spread, is shown in Fig. 12. Curve A refers to values obtained from the above binding field equation and curve B to the results of analyses which take into account the above mentioned input coupler effects. This comparison presents a rather pessimistic outlook for narrow phase width performance at moderate currents and low gun potentials, unless the velocity spread at injection is very low, and it provides a possible explanation of the common observance that a small change of prebuncher drive affects the beam energy spectrum far more than predicted by the simple binding field theory.

The Table 7 and Fig. 12 data refer to phase spreads between single particles injected at the same phase but with different energies. The Fig. 13 curves show typical emergent phase angles (δ) for a 7 MeV buncher waveguide, for different entry phase angles (ϕ_0) at the input coupler fringe field, and for three closely related injection energies. These data also relate to single particle injection and include the effects of input coupler space harmonics. (In practice, for a high duty cycle machine, the buncher waveguide would be designed for a lower emergent phase angle to allow for reduced gradient operation and the effects of beam loading.) Single particle phase plots of this nature are not directly applicable, however, to the phase orbital behavior of individual particles in a cohesive bunch. Therefore, the concept of exploiting the ΔV_0 separation of these curves to produce a narrow emergent phase spread, by injecting a prebunched beam so that early particles of low energy emerge at a low value of δ, thereby enabling the late entry, higher energy particles to advance in phase, cannot be validly applied. Electron bunching analyses which take into account the effects of reactive phase shift (see section 2.5.3) and space charge, due to beam loading, indicate that the phase orbital characteristics of intra-bunch particles are unlike those of the Fig. 13 ballistic derived curves. As an example, the broken curve superimposed on the Fig. 13 data shows the emergent phase width for the hypothetical case of a 25 mA, 12 degree bunch injected with uniform charge density at an energy of 400 keV. The emergent phase spread is increased due to a "rotation" effect, caused mainly by the influence of space charge and migration within the bunch, during passage through the initial portion of the circuit. For short bunches, these phase characteristics appear to be affected most by phase location of the centroid, phase width at injection, total charge and beam diameter. (Under some circumstances, a highly compressed bunch with a narrow injection phase spread can result in a broadening of the emergent phase angle.) Although each beam loading condition has to be analyzed separately, in general, the achievement of a narrow emergent phase spread depends on, not only satisfying the stringent $\Delta\beta_0$ injection requirements discussed above, but also on maintaining the bunch in a sufficiently high field gradient to counteract the effects of space charge (see section 2.5.4).

The above conclusions, pessimistic as they appeared for the case of a narrow emergent bunch, were influential in establishing the injector beam specifications and evaluating various injection systems. The eventual selection of a high energy, chopper-prebuncher system was based on a buncher waveguide injection requirement of a bunch phase width between 5 and 10 degrees and a maximum velocity spread of ± 0.4 percent of c, to achieve a total phase,width at emergence of not greater than 2 degrees with peak current values up to 25 mA.

6.2 Selection of Gun Potential and Drift Space Parameters

Since the biased chopper-prebuncher principle has been presented in earlier reports and discussed in connection with a variety of previously constructed machines†, it will be assumed that the reader is familiar with this means of obtaining a well-defined RF bunch of adjustable phase width. When 120 degrees of beam length per RF cycle ($\beta_0 \lambda_0/3$) is correctly phased to traverse the prebuncher gap during field reversal, the electrons will be subjected to velocity modulating fields which closely approximate the ideal saw-tooth environment required for linear bunch compression in the subsequently located drift space in the absence of space charge. (For biased-chopper operation, this results in a transmission efficiency of approximately 20 percent.) If, for the present, we disregard the effects of radial and longitudinal space charge fields, then the total $\Delta\beta_0$ and ΔV_0 that must be introduced by the prebuncher-gap, for bunch compression

from 120 to 10 degrees over a given drift space length S, can be determined from the simple time-of-flight expression[27]

$$(\phi_2 - \phi_0) = \phi_1 + 2\pi S\,[(\beta_0/\beta_m) - 1]/(\beta_0 \lambda_0)$$

where ϕ_1 and $(\phi_2 - \phi_0)$ are the departure and normalized arrival phases, respectively, and $\beta_0 c$ and $\beta_m c$ are the velocities of the unmodulated and modulated electrons, respectively. [The electron energy (V_m in keV), as obtained for a given prebuncher gap condition and departure phase, can be related to its velocity by $(V_m/511) + 1 = (1 - \beta_m^2)^{-1/2}$.] Furthermore, by imposing a restriction based on practical requirements, namely, that for variations of gun potential of ± 0.1 percent the phase modulation at the end of the drift space shall be no greater than ± 1.5 degrees, then the maximum permissible drift length will be defined by the gun potential. The relationship is developed in section 2.5.1 and, for the above voltage variation, may be written as $\Delta\phi_s = 2\pi S\, 10^{-3}\,(\gamma - 1)(\gamma^2 - 1)^{-3/2}/\lambda_0$, where $\Delta\phi_s$ is the permissible phase modulation at the end of the drift space, and γ is defined by the energy of the source electrons. The values of S, $\Delta\beta_0$ and ΔV_0, as obtained from the above equations for a range of beam energies up to 500 keV, are shown in Fig. 14. These curves show that for systems operating at low beam energies, quite small values of total energy spread ($\Delta V_0 < 10$ keV) result in 12 to 1 bunching, but these values are accompanied by large spreads in velocity ($\Delta\beta_0 > 1.5$ percent). As the gun potential increases, however, the larger values of drift space and energy spread are accompanied by reduced values of velocity spread.

If now space charge effects are taken into consideration, it is evident that bunch terminal field strengths of less than 1 kV/cm, acting over a few centimeters, will, for the lower beam energies, seriously perturb the bunching process. To determine the importance of space charge effects which counteract the velocity modulation produced by the prebuncher, we can consider the commonly adopted drift space configuration in which the beam waist is located at the prebuncher, and after velocity modulation, the bunch is allowed to expand freely before passing through a thin lens assembly and refocusing through a small aperture at the end of the drift space. Thus, toward the end of the drift space, the bunch dimensions are reduced both in the longitudinal and radial direction. For low beam energies, and moderate currents, to overcome the high space charge forces generated by this volume compression, it is essential that the drift space lengths shown in Fig. 14 be drastically reduced and the prebuncher drive be increased. At higher beam energies, not only are the space charge forces reduced, but the higher values of ΔV_0 required for bunching can more readily dominate the space charge potentials. It should be noted that, for high duty factors machines, lower values of perveance allow the beam to be expanded over a larger proportion of the drift length prior to refocusing (see Fig. 16), i.e., the radial compression occurs over a proportionally shorter length of drift space. For a given operational condition, to assess de-bunching effects due to space charge, and prior to considering the results of detailed computations, a reasonable estimate of gross effects can be made by selecting a suitable bunch model and determining the maximum value of longitudinal field strength. For example, Fig. 15(b) shows the relationship between maximum longitudinal field and bunch length for a constant diameter bunch and several values of beam energy. (A spheroidal bunch model of non-uniform charge density [see Fig. 15(a)] was chosen as a good approximation to practical conditions as determined by profilometer and RF bunch sweeping[6] measurements.) The Fig. 15(b) curves indicate that, with a 2 mm diameter, 100 keV beam, any attempt to bunch 25 mA into 5 or 10 degrees over a distance of several centimeters would result in much larger de-bunching potentials than the prebuncher ΔV_0 values of Fig. 14. Of course, the prebuncher drive could be increased and the drift space foreshortened at this lower injection voltage;[27] but under these conditions, the correct compensation of space charge forces becomes a very sensitive function of beam current and lens settings, and prevention of longitudinal phase orbit crossovers, an important requirement for optimum bunching in subsequently located waveguide, cannot be assured.

On the other hand, with a 400 keV beam of the same diameter, the Fig. 15(b) data indicates that bunching down to 5 or 10 degrees over relatively long distances would result in space charge potentials much lower than the ΔV_0 prebunching value shown for this higher injection energy in Fig. 14. Under these conditions, because of the dominance of the prebuncher drive, accurate compensation of space charge fields no longer plays an important role in obtaining a small bunch width, and it can be expected that high voltage systems of this type will be relatively insensitive to different settings of beam current. Furthermore, because of the low perveance and linear compression characteristics, reliance can be placed on the reproducibility of the space charge fields and the associated partial cancellation of the $\Delta\beta_0$ initially introduced by the prebuncher. This cancellation assists in satisfying the buncher waveguide requirement for a narrow spread of injection velocities.

The above considerations, supported by the results of detailed space charge analyses in the drift space region, led to the conclusion that a high beam energy chopper-buncher system would meet the stringent injection conditions required by the buncher waveguide in order to demonstrate an emergent bunch width at less than 2 degrees.

6.3 Injection Layout and Results of Analyses

A schematic layout of the injection system is shown in Fig. 16. Detailed calculations in radial and longitudinal phase space in the drift length region, including space charge effects, were conducted over a wide range of parameters; and some results corresponding to the Fig. 16 positions marked A, B and C are reproduced in Fig. 17. These data refer to a 25 mA, 400 keV bunched beam with an initial geometry and non-uniform charge density distribution, as shown in Fig. 15(a), an initial and final diameter of 2 mm, an initial biased-chopped bunch length of 2.9 cm (120^o of $\beta_0 \lambda_0$ at 2856 MHz), a prebuncher peak field strength of 18.5 kV/cm, and a 850 gauss lens 91 cm from the prebuncher. The bunch was divided into a multiplicity of cylindrical and annular elements, the boundaries and centroids of which can be seen in the Fig. 17 illustrations. This technique, which has been described elsewhere,[28] assumes that rotational symmetry is conserved about the beam centerline and that the charge density distribution in the azimuthal direction remains constant.

The Fig. 17 results indicate that, after 132 cm of drift, a bunch length of 118 degrees at the prebuncher departure plane is reduced to 9 degrees, and the total ΔV_0 is reduced correspondingly from 29.1 to 18.5 keV, i.e., the total $\Delta\beta_0$ is reduced from 1.2 to 0.8 percent of c. At this point, while the regular pattern of annulii has been disturbed due to non-linearities, the maximum space charge longitudinal field is less than 0.5 kV/cm. Further bunching occurs with increasing drift distance. Data taken at 140 cm indicate that the total phase width is reduced to 5 degrees, and with the increasing space charge fields, total ΔV_0 and $\Delta\beta_0$ are decreased to 12 keV and 0.5 percent of c, respectively. These results suggested that the narrow phase width and velocity spread requirements at injection into the buncher waveguide, as specified in section 6, could be satisfied by this concept and, in fact, that care should be taken to avoid compression of the bunch to too small a phase width, especially at high duty cycle, because of an incompatibly low field gradient in the buncher waveguide.

The Fig. 18 phase orbit data shows the computed phase spread emergent from the buncher waveguide (see Fig. 16, position D), for the input RF conditions listed in Fig. 13, and an injected electron bunch with a non-uniform charge density and velocity distribution as obtained from the Fig. 17 drift space computations.

Acknowledgments

The author gratefully acknowledges the valuable contributions and assistance of Miss Beverly Mecklenburg, particularly during the conceptual and design stages of the high power microwave structures and injection system for the MIT accelerator, and, the diligent and able assistance of Mr. Otto H. Altenmueller in conducting microwave measurement programs on large iris aperture structures. The author is also indebted to colleagues, at both SLAC and MIT, for their stimulating and helpful discussions and, in addition, takes this opportunity to express his gratitude to the publication staff at SLAC for their cooperative efforts in preparing this (and other) documents.

References

1. A. Sokolovsky, Proc. LASL Linac Conference, Los Alamos, New Mexico, 417 (1966).
2. H. Leboutet et al., Proc. LASL Linac Conference, Los Alamos, New Mexico, 426 (1966).
3. W. Bertozzi et al., IEEE Trans. Nucl. Sci. 14, 191 (1967).
4. P. B. Wilson, in Linear Accelerators, ed. by P. Lapostolle and A. Septier, to be published (1968).
5. H. A. Schwettman et al., IEEE Trans. Nucl. Sci. 14, 336 (1967).
6. J. Haimson, IEEE Trans. Nucl. Sci. 12, 996 (1965).
7. R. B. Neal, Report No. ML513, Microwave Laboratory, Stanford University, Stanford, California (1958).
8. P. N. Robson, Proc. IEE 105B, 69 (1958).
9. "Two-mile accelerator project, Quarterly Status Report, 1 April to 30 June 1964," SLAC Report No. 32, Stanford Linear Accelerator Center, Stanford University, Stanford, California (1964).
10. J. Haimson, Nucl. Instr. and Methods 33, 93 (1965).
11. J. E. Leiss, IRE Trans. Nucl. Sci. 12, 566 (1965).
12. G. Saxon and J. White, Proc. IEE 3, 465 (1964).
13. R. Jean, L'Onde Electrique, 435 Vol. XLIII, 623 (1963).
14. E. A. Knapp et al., Proc. LASL Linac Conference, Los Alamos, New Mexico, 83 (1966).
15. R. Bergere and A. Veyssière, Nucl. Instr. and Methods 30, 309 (1964).
16. L. Burnod, L'Onde Electrique, 435 Vol. XLIII, 688 (1963).
17. Z. D. Farkas et al., IEEE Trans. Nucl. Sci. 14, 223 (1967).
18. J. Weaver and R. Alvarez, IEEE Trans. MTT 14, 623 (1966).
19. J. Haimson and L. Katz, IEEE Trans. Nucl. Sci. 12, 457 (1965).
20. R. B. Neal and W.K.H. Panofsky, Science 152, 1353 (1966).
21. R. Helm, Proc. LASL Linac Conference, Los Alamos, New Mexico, 254 (1966).
22. G. A. Loew, IEEE Trans. Nucl. Sci. 14, 529 (1967).
23. O. H. Altenmueller et al., Proc. LASL Linac Conference, Los Alamos, New Mexico, 267 (1966).
24. J. Haimson and I. Brodie, Nature 199, 795 (1963).
25. M. Chodorow et al., Rev. Sci. Instr. 26, 134 (1955).
26. J. Haimson, Nucl. Instr. and Methods 39, 13 (1966).
27. J. Haimson, IRE Trans. Nucl. Sci. 9, 32 (1962).
28. J. Haimson and B. Mecklenburg, IEEE Trans. Nucl. Sci. 14, 586 (1967).

Footnotes

* Work supported by the U.S. Atomic Energy Commission.

**In general the cold stack values of r and I, as obtained from mechanically clamped components, are improved by several percent after final assembly and brazing, due to an enhancement of the waveguide Q which is dependent on the copper annealing process and type of braze material used.

† Particle Accelerator Conference, Washington, IEEE Vol. NS-12, pp. 459 and 501, (June 1965), and Proceedings 1966 Linear Accelerator Conference at Los Alamos, p. 331 (October 1966).

TABLE 1. Microwave Design Data for $2\pi/3$ Mode, $v_p = c$, 2856 MHz Waveguide

Iris Diameter		Inspection Dimensions B"(±0.0005)				Cylinder* Diameter 2b"(±.0002)	Group† Velocity v_g/c	Shunt Impedance r Meg Ω/m	Attenuation Constant I neper/m
2a"(±.0002)	2a(cm)	D_B = 1.0000"	1.2500"	1.5000"	1.7500"				
0.7000	1.7780	0.7846	1.0831			3.2078	0.0048	59.35	0.489
0.7500	1.9050	0.7537	1.0618			3.2164	0.0061	58.30	0.376
0.8000	2.0320	0.7181	1.0386			3.2257	0.0079	57.30	0.288
0.8500	2.1590	0.6763	1.0131	1.3082		3.2365	0.0100	56.25	0.225
0.9000	2.2860		0.9849	1.2873		3.2482	0.0124	55.15	0.179
0.9500	2.4130		0.9537	1.2648		3.2605	0.0151	54.10	0.146
1.0000	2.5400		0.9185	1.2405		3.2744	0.0181	53.00	0.120
1.0500	2.6670		0.8785	1.2140	1.5127	3.2900	0.0215	52.05	0.100
1.1000	2.7940		0.8317	1.1852	1.4907	3.3060	0.0254	51.05	0.084
1.1500	2.9210			1.1537	1.4671	3.2427	0.0295	50.10	0.072
1.2000	3.0480			1.1188	1.4419	3.3397	0.0340	49.00	0.062
1.2500	3.1750			1.0799	1.4147	3.3573	0.0389	48.00	0.055

All dimensions at 24°C.

*Includes an allowance for hydrogen brazing and slight tuning compression to provide 2856 MHz at 45°C in vacuum.

†Obtained from a Fourier series representation of the dispersion curve.

TABLE 2. Comparison of System Parameters at Different Duty Factors

Beam Duty Factor (%)	Klystron Rated Peak Power (MW)	Klystron Rated Average Power (kW)	Number of Klystrons	System Total Average Power (kW)	Waveguide Sections per Klystron	Total Number of Sections	Waveguide (τ = 0.82) Section Length (m)	Total Length of Waveguides (m)	Unloaded Beam Energy (MeV)	Beam Duty Factor (%)	Peak Current (mA) to give 150 μA Average Current	Loaded Beam Energy at 150 μA Average (MeV)
0.1	20	25	6	150	2	12	5.04	60.5	545	0.1	150	403
1.8	4.0	80	7	560	4	28	7.35	206	452	1.8	8.4	400
1.8	4.0	80	9	720	2	18	7.35	132	422	1.8	8.4	405
4.8	1.5	80	7	560	4	28	7.35	206	276	4.8	3.1	266
4.8	1.5	80	9	720	2	18	7.35	132	258	4.8	3.1	251
5.8	1.0	65	7	455	4	28	7.35	206	226	5.8	2.6	217
5.8	1.0	65	9	585	2	18	7.35	132	211	5.8	2.6	205

TABLE 3. Energy Spectrum Dependence on Duty Factor and Beam Loading

Input Coupler RF Power P_o(MW)	Waveguide Sections per Klystron	Waveguide Length ℓ(m)	Energy Gain per Section V(MeV)	Beam Duty Factor (%)	Peak Current for 150 μA Average Current i(A)	Tolerable (Δi/i) at 150 μA Average Current for 0.1%(ΔV/V) (%)	Tolerable ($\Delta P_o/P_o$) at 150 μA Average Current for 0.1%(ΔV/V) (%)	Tolerable ($\Delta V_k/V_k$) at 150 μA Average Current for 0.1%(ΔV/V) (%)
9.80	2	5.04	(45.4-79i)	0.1	0.1500	0.28	0.148	0.060
0.85	4	7.35	(16.2-118i)	1.8	0.0084	1.53	0.187	0.071
1.80	2	7.35	(23.5-118i)	1.8	0.0084	2.27	0.191	0.077

TABLE 4. Principal Design Parameters of the Saclay (ALS) Accelerator

Number of klystrons	15 (type TV 2013)
Number of modulators	7 driving 2 klystrons each 1 driving No. 1 klystron
Number of waveguide sections	30
Overall electrical length	170 meters
Klystrons	
Operating frequency	2998 MHz
Peak RF power (nominal)	4 MW and 2 MW
Average RF power	60 kW and 60 kW
Microperveance	2.0 ± 0.1
Peak beam voltage	140 kV
Efficiency	$\geq 35\%$ at 4 and 2 MW
Gain	≥ 46 dB
Dual RF output through ceramic windows into pressurized waveguide	
Modulators (Hard Tube)	
Peak power	12 MW at 1 kHz, 6 MW at 2 kHz
Average power	180 kW
Peak voltage	140 kV
Peak current	91.5 A
Load dynamic impedance	1350 to 1550 ohms
Switch tubes	Two CSF-F 6046 rated 40 kV
Capacitor bank	3.75 μF
Crowbar protection	Maximum energy release 800 joules Maximum energy current 1000 A
Pulse duration (99.5% flat-top)	11.2 ± 0.2 μsec
Voltage pulse flat-top specification (total) at any point between 9.4 and 11.8 MW or 4.6 and 5.8 MW:	
Without retouching	$\pm 0.5\%$
At any point after adjustment	$\pm 0.125\%$
Pulse repetition rate	1 kHz and 2 kHz
RF duty factor	1.1% and 2.2%
Drive System	
Master oscillator using a stabilized CW reflex klystron to drive first high power klystron. Signal coupled from output of first klystron drives 14 remaining klystrons through a coaxial line.	
Main Waveguide Sections (No. 3 through 30) $2\pi/3$ mode	
Length	6 meters (except No. 7 which is 3.2 meters for high gradient following positron converter)
Number of cavities	179
Number of segments per waveguide	7
Disc thickness	3 mm with a $60° \times 12$ mm chamfer onto cylinder
Attenuation parameter	0.7 neper
Shunt impedance range	56 to 70 megohms per meter
Group velocity range	0.036 to 0.012 v_g/c
Filling time	1.04 μsec
Average Q	14,000
Zero current energy gain	22 MeV at $P_o = 1.8$ MW
Beam pulse length	10 μsec
Beam duty factor	1% and 2%
Cooling	10 pipes $\times$ 12 mm I.D.
Water flow per section	3 liters per sec
Construction	Silver diffusion braze and vacuum jacket
2200 gauss solenoids on sections after positron converter	
Injector	
Chopper - prebuncher and tapered phase velocity buncher in series-connection with a 2.6-meter section	
Electron gun microperveance	10^{-2}
Electron gun voltage	50 kV
Injected bunch width	20 degrees
Buncher length	1.8 meters
Buncher zero current energy gain	6.25 MeV at $P_o = 1.4$ MW
Beam emittance measured at 6 MeV and 40 mA	3×10^{-3} rad $\times$ cm
Energy spread measured at end of buncher at 30 mA	50% current in 1.3%
Overall Performance Specification	
Zero current total beam energy	554 MeV at 1% duty, 380 MeV at 2%
Beam energy at 20 mA	500 MeV (1% duty)
Beam energy at 15 mA	340 MeV (2% duty)
Energy spread	50% current in 1%

TABLE 5. Principal Design Parameters of the MIT Accelerator

Number of klystrons	10 (type VA 938)
Number of modulators	5 each driving two klystrons
Number of waveguide sections	24
Overall electrical length	150 meter
Klystrons	
Operating frequency	2856 MHz
Microperveance	2.0 ± 0.1
Peak RF power (nominal)	4 MW to 1 MW
Average RF power	80 kW to 65 kW
Beam voltage	130 kV to 80 kV
Minimum efficiency	35% to 30%
Minimum gain for saturation	41 db
Single RF output through ceramic window into pressurized waveguide	
Modulators (Hard Tube)	
Peak power	23 MW at 1.25 kHz, 7 MW at 4 kHz
Average power	520 kW
Peak voltage	140 kV
Peak current	200 A
Load dynamic impedance	1400 to 1700 ohm
Switch tubes	Four Litton – L5097 rated 180 kV
Capacitance bank	1.8 μF
Crowbar protection	Maximum energy release < 50 joule
Pule duration (99% flat-top)	Continuously variable up to 15 μsec in accordance with duty factor and peak power (see Fig. 8)
Voltage pulse flat-top specification	$\pm$ 0.15%
Pulse repetition rate	Continuously variable up to 5 kHz in accordance with duty factor and peak power (see Fig. 8)
RF duty factor	2% to 6.5%
Drive System	
Master driver consisting of a crystal controlled solid state oscillator and a 1 kW CW klystron with optional pin-diode modulation for pulsed output. Main coaxial drive line serves five 1 kW klystrons (using regulated dc power supplies), each of which drives two main klystrons.	

Main Waveguide Sections (4 short and 18 long) $2\pi/3$ mode, approx. constant gradient			
Length	3.675	and	7.35 meter
Number of cavities	105	and	210
Disc thickness	5.84	and	5.84 mm
Number of uniform segments per section	11	and	11
Range of shunt impedance	53.8 – 57.7	and	48.0 – 56.5 MΩ/m
Range of group velocity (v_g/c)	0.0156 – 0.007	and	0.0389 – 0.0093
Average attenuation parameter	0.75	and	0.825 neper
Average Q	13400	and	13750
Filling time	1.12	and	1.27 μsec
Zero current energy gain at P_o = 1.8 MW	16.6 MeV	and	23.2 MeV
Zero current energy gain at P_o = 0.8 MW			15.5 MeV
Beam pulse length	Variable up to 14 μsec in accordance with duty factor and peak RF power.		
Beam duty factor	1.8% at P_o = 4 MW and 5.8% at P_o = 1 MW		
Cooling	12×11 mm I. D. and 8×16 mm I. D. tubes		
Water flow per section	6.3	and	6.3 litre per sec.
Construction	Hydrogen braze (copper-silver eutectic) and vacuum jacket		
Steering coils at each input coupler, no solenoids for long sections.			
Injector Design			
Biased chopper – prebuncher and high gradient buncher in series – connection with a 3.7 meter section			
Electron gun microperveance	10^{-3}		
Electron gun voltage	300 – 400 kV		
Injected bunch width	< 10 degrees		
Buncher length	1.2 meter		
Buncher zero current energy gain	6.9 MeV at P_o = 2.5 MW		
Beam emittance design specification at 6 MeV	$10^{-3} \pi m_o c \times cm$		
Overall Performance Specification			
Zero current total beam energy	430 MeV at 1.8% duty		
Beam energy at 10 mA	400 MeV at 1.8% duty		
Energy spread	50% current in $\pm$ 0.2%		

TABLE 6. MIT Waveguide Computed HEM_{11} Resonances (Three Segments Only)

Group	First Segment		Second Segment		Third Segment	
	2a"	f(MHz)	2a"	f(MHz)	2a"	f(MHz)
AA	0.9600	4198.4 4214.5 4241.0	0.9433	4208.3 4217.0 4228.0	0.9295	4220.0 4228.2 4239.6
BB	0.9600	4192.7 4198.0 4203.8 4210.0	0.9433	4209.2 4219.8 4232.2	0.9295	4221.0 4231.2 4244.2
A	1.2500	3948.0 3948.8 3950.3 3952.4 3955.2	1.2369	3957.9 3958.6 3959.7 3961.3 3963.6	1.2185	3972.4 3973.2 3974.5 3976.3 3978.8
B	1.2083	3980.7 3981.6 3983.1 3985.3	1.1964	3990.4 3991.4 3993.2 3995.7	1.1891	3996.6 3997.6 3999.0 4001.3
C	1.1735	4010.0 4011.2 4013.0 4015.4	1.1539	4026.6 4028.0 4030.4 4033.7	1.1452	4033.9 4035.2 4037.5 4040.7
D	1.1378	4040.3 4041.8 4044.4 4047.8	1.1208	4054.6 4059.1 4062.7 4067.2	1.1115	4062.4 4063.8 4066.7 4069.8

TABLE 7. Permissible Energy and Velocity Spread Versus Asymptotic Phase Spread* for Injection at $\delta_0 = 0$ Into $v_p = c$ Waveguide

V_0	E_0	Energy Spread ΔV_0(keV)		Velocity Spread $\Delta\beta_0$	
keV	kV/cm	For $\Delta\delta_a = 1^o$	For $\Delta\delta_a = 2^o$	For $\Delta\delta_a = 1^o$	For $\Delta\delta_a = 2^o$
100	165	6.0 (2.5)	12.3 (5.0)	.0122 (.0052)	.0244 (.0102)
200	130	8.8	18.0	.0090	.0179
400	94	13.4 (9.8)	27.4 (19.5)	.0055 (.0040)	.0109 (.0078)

*This does not include phase spread effects due to space harmonics, fringe field or presence of charge.

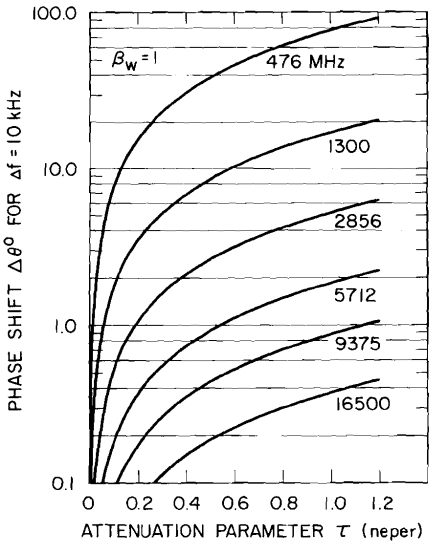

1. Relationship between waveguide phase shift and attenuation parameter.

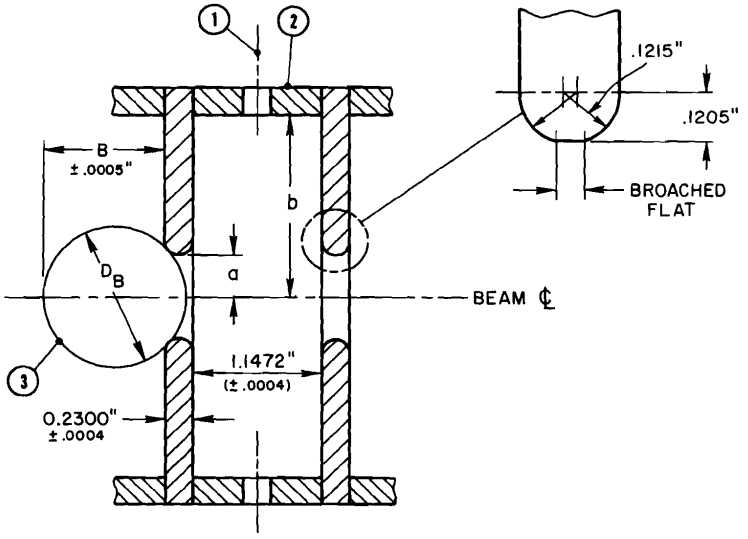

Notes:

1. 8-Holes Reamed 0.196" Dia. 30°/60° Azimuthal Spacing
2. Spacer Silver Plated (O.D. and Ends)
3. Ground Steel Ball for Iris Contour Inspection
4. Internal Surface Finish Less than 14 Microinches
5. All Dimensions at 24° C
6. Material: Annealed Certified OFHC Copper

2. Cavity details for $2\pi/3$ mode, $v_p = c$, 2856 MHz waveguide.

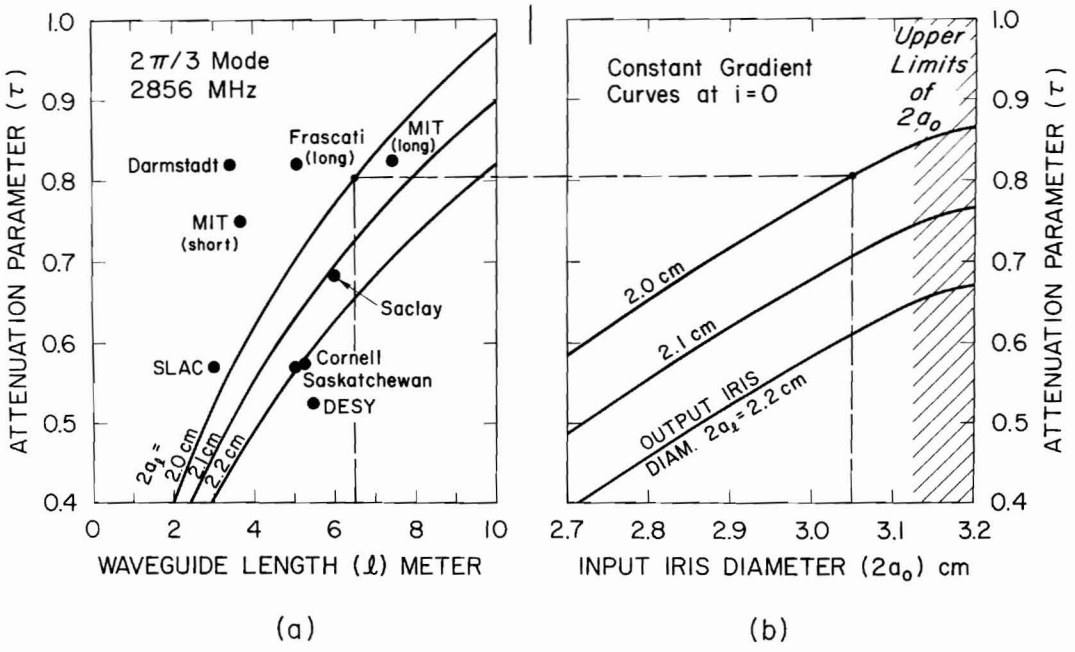

3. Constant gradient waveguide relationship between attenuation parameter, length and iris diameter.

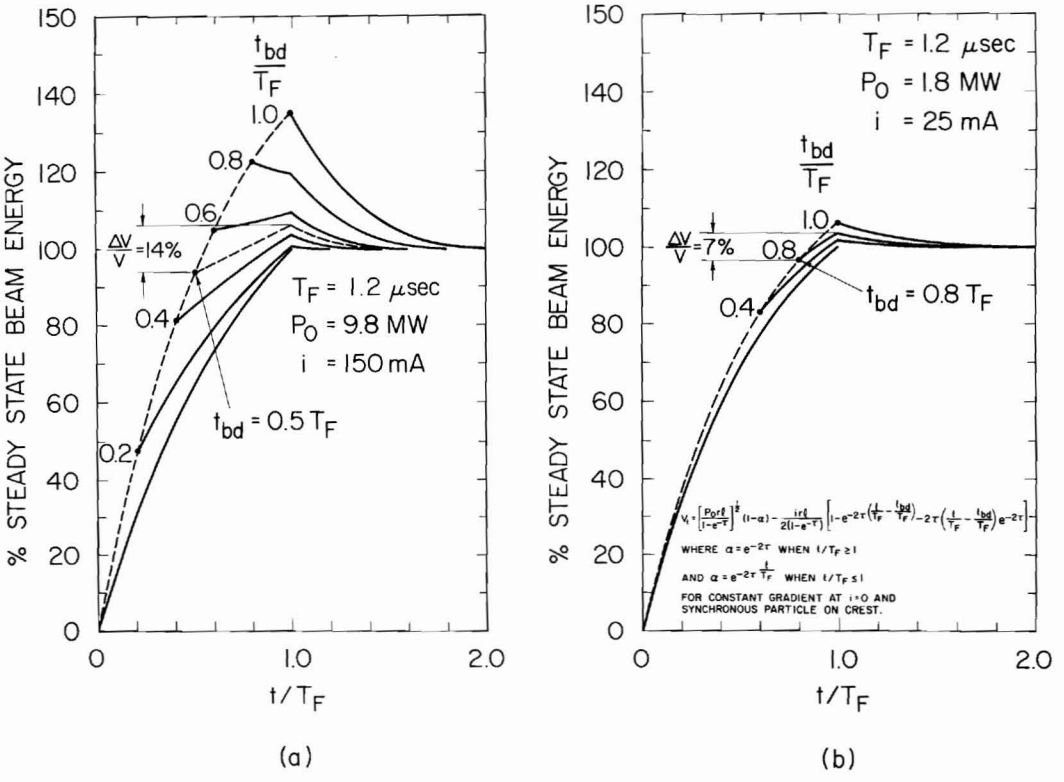

4. Beam loading transient characteristics.

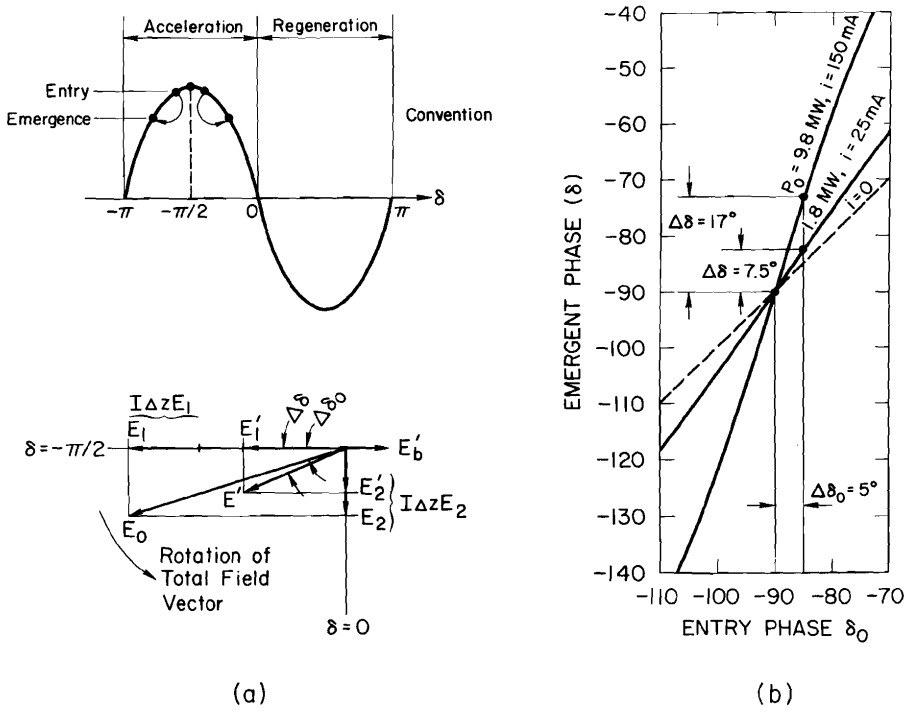

5. **Reactive phase shift effect.**

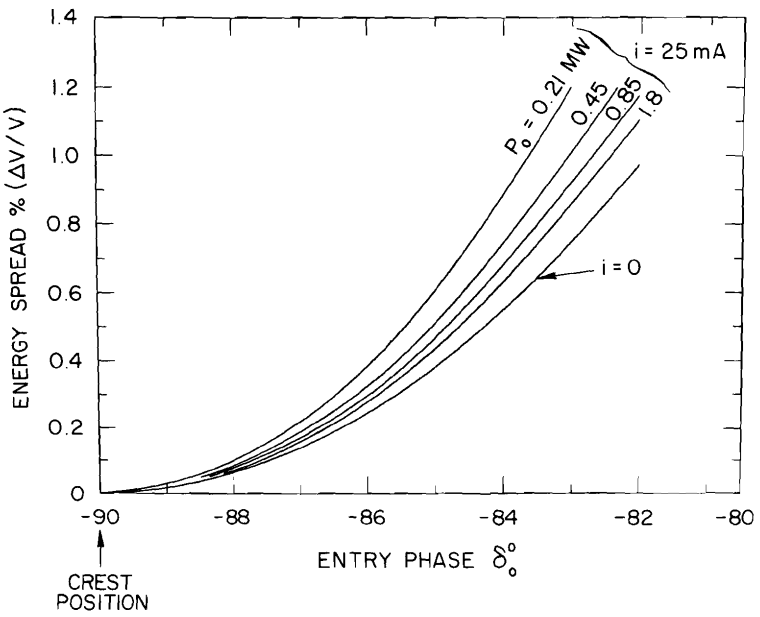

6. **Energy spread due to finite bunch width and reactive phase distortion.**

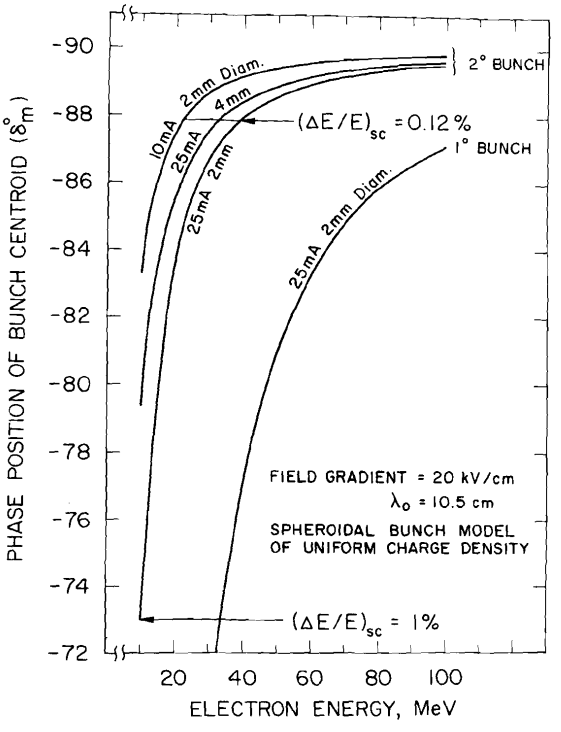

7. **Phase position to cancel space charge energy spread.**

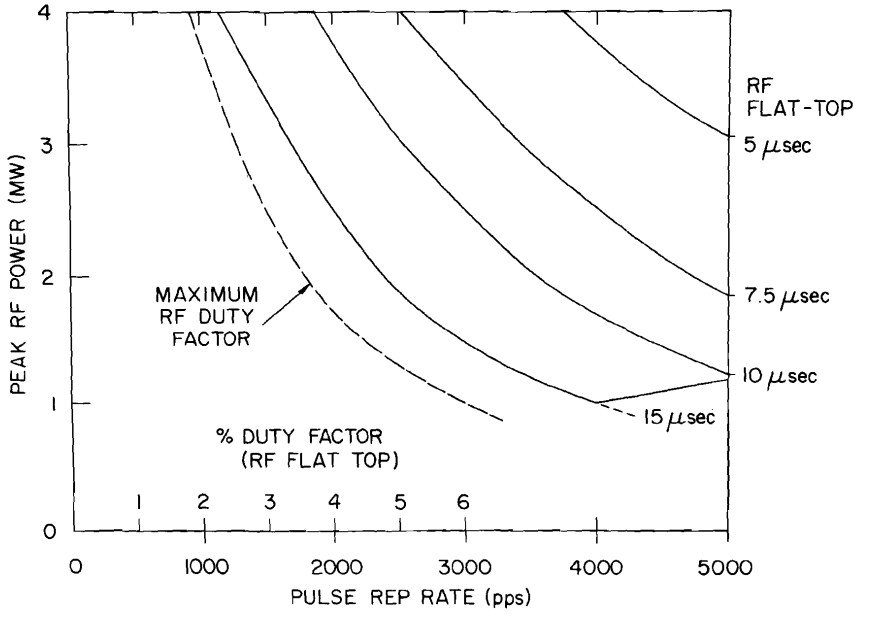

8. **RF transmitter high duty factor pulse parameters.**

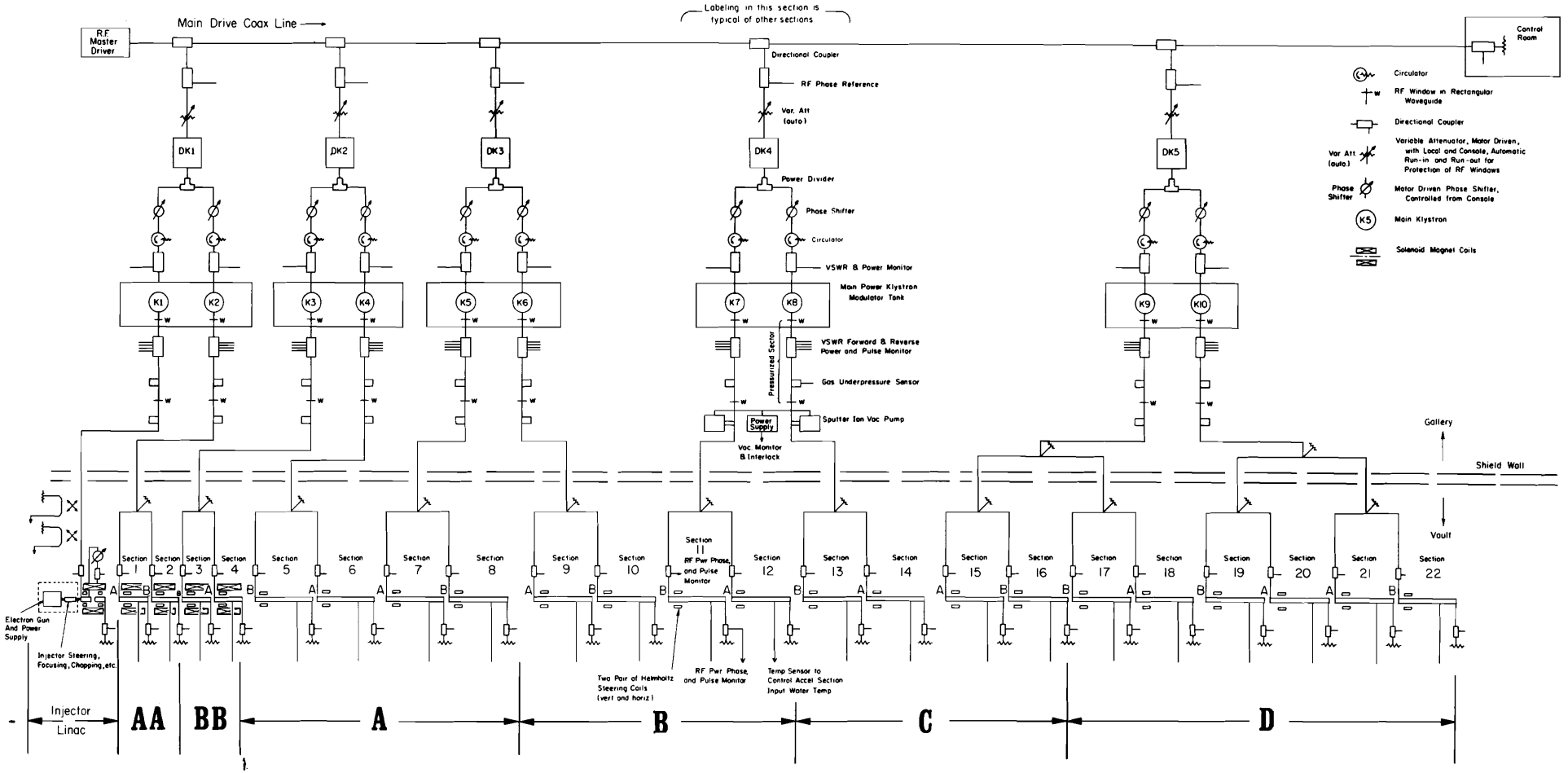

9. Schematic layout at the MIT 400-MeV linear accelerator.

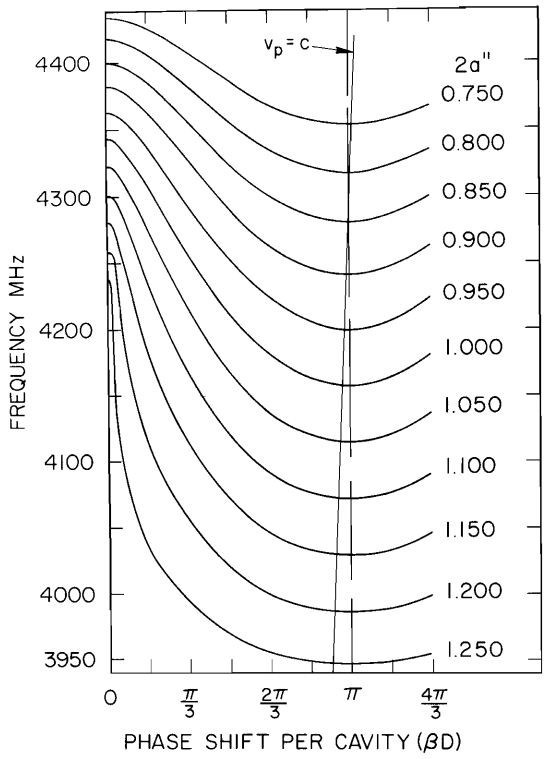

10. Typical Brillouin diagrams for the HEM_{11} mode.

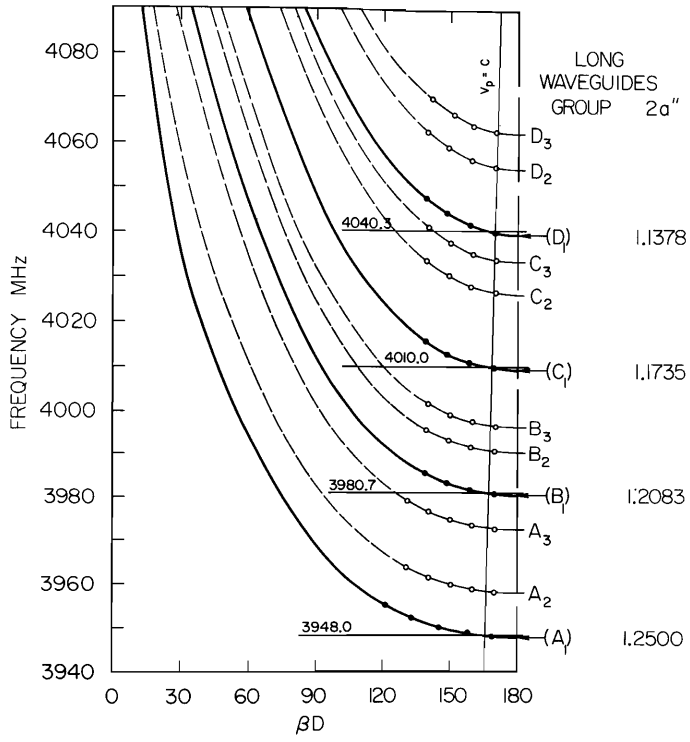

11. HEM_{11} mode Brillouin diagrams indicating progressive stop-band separations.

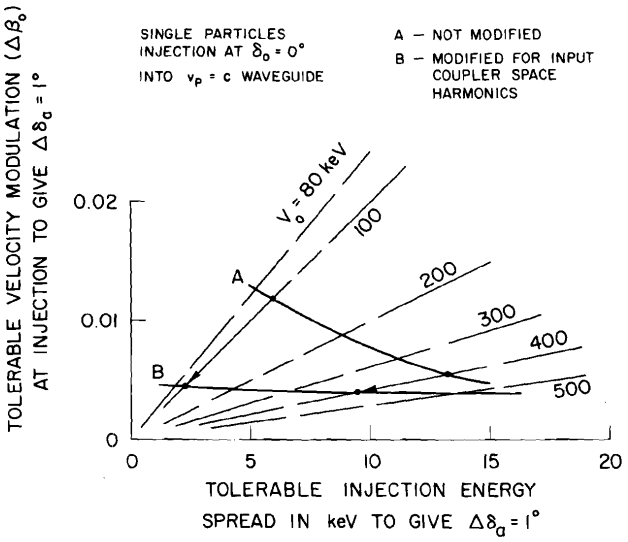

12. Effect of space harmonics on tolerable velocity spread at injection.

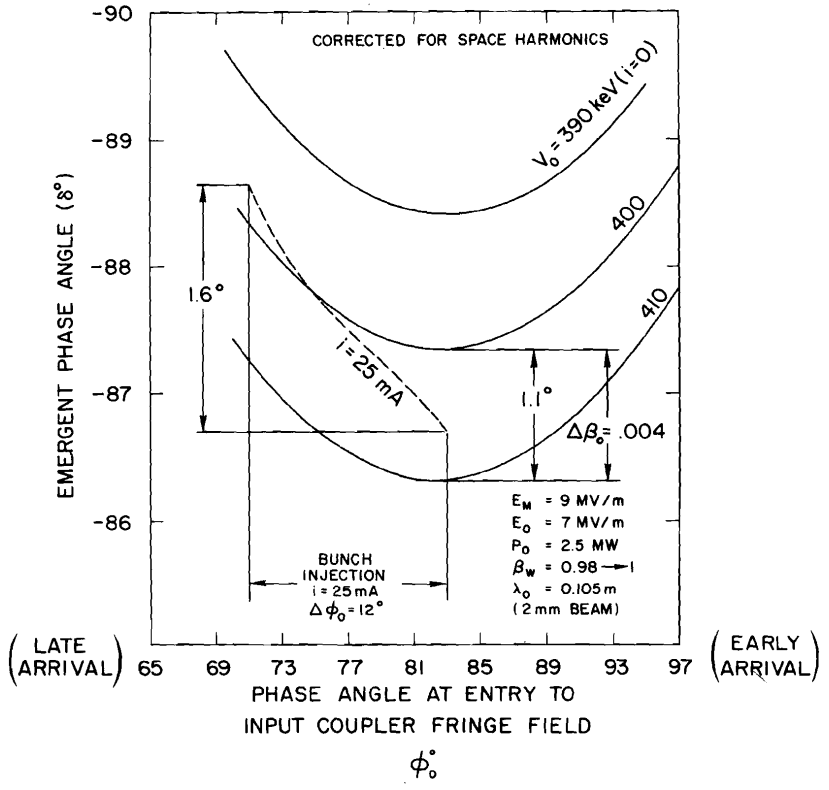

13. Space harmonic corrected phase orbit plots for an unloaded buncher waveguide.

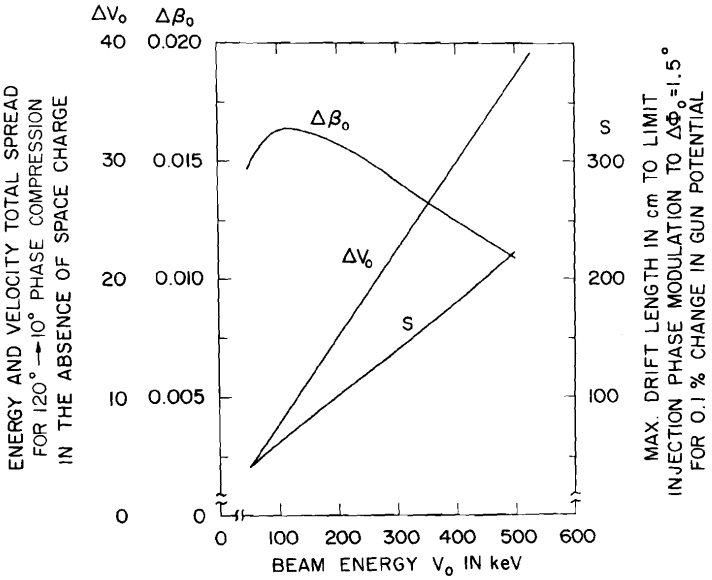

14. Drift space parameters in the absence of space charge.

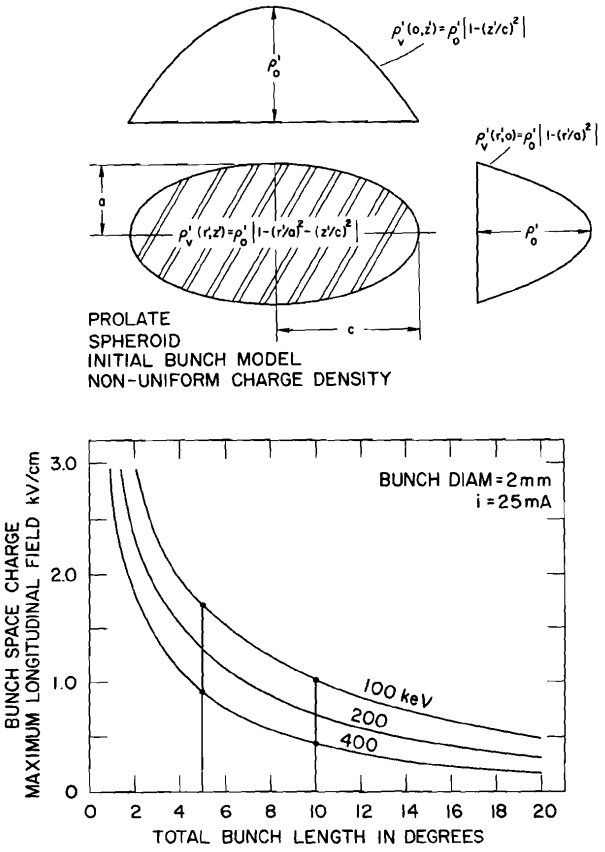

15. Space charge maximum longitudinal field for non-uniform charge density spheroidal bunch.

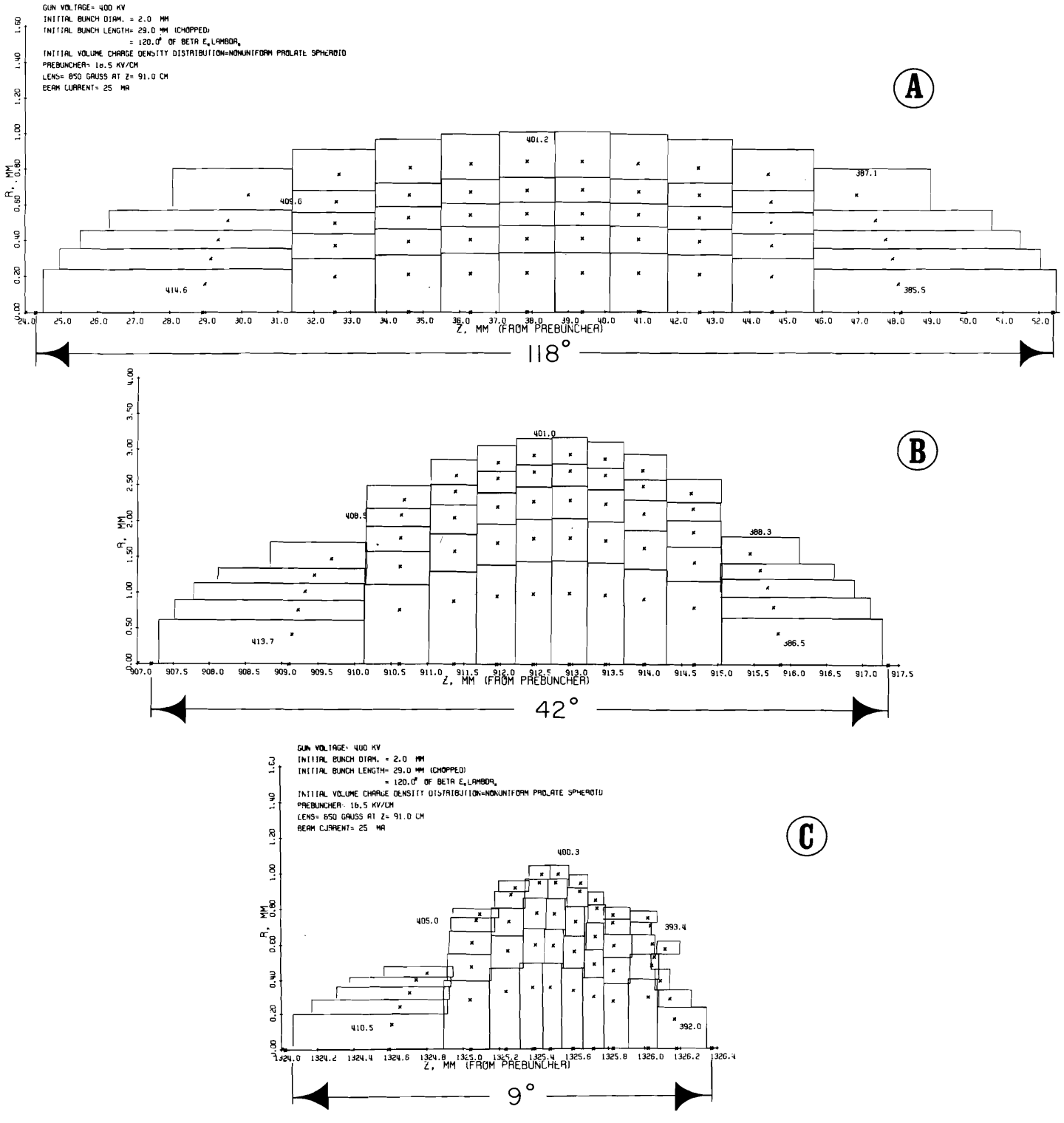

16. Schematic layout of injection system.

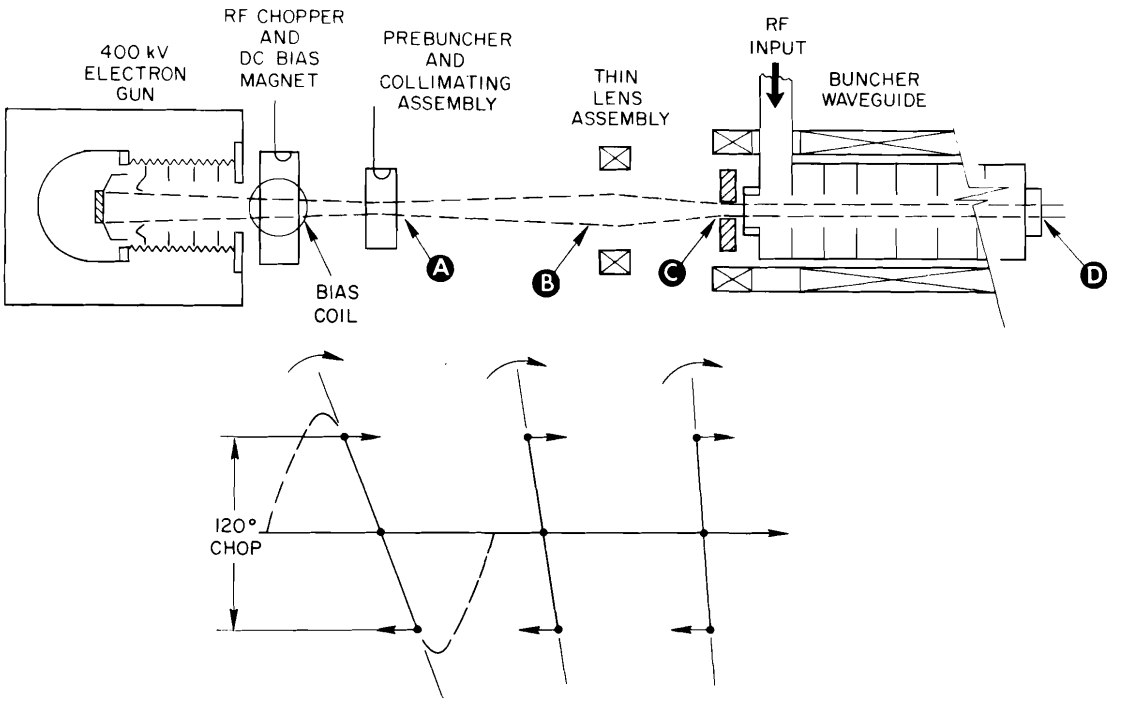

17. Drift space bunch compression corrected for space charge effects.

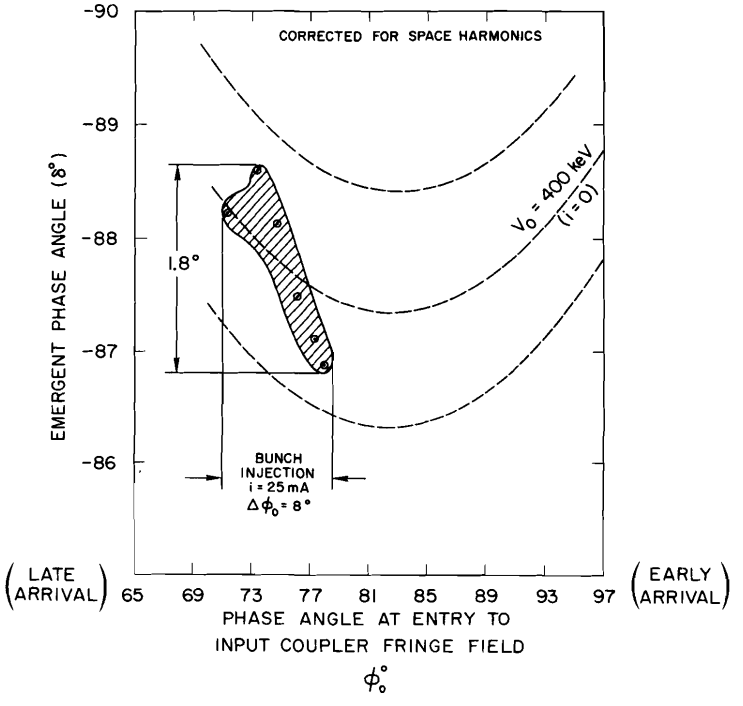

18. Buncher waveguide phase orbit plots for an injected narrow bunch and 25 mA loading.